Legendre Moments Explorations via Image Reconstruction

by

Pei-Jung Amy Chiang

A Thesis

Submitted to the Faculty of Graduate Studies

in Partial Fulfilment of the Requirements

for the Degree of Master of Science

Department of Applied Computer Science

University of Winnipeg

Winnipeg, Manitoba, Canada

Copyright© Pei-Jung Amy Chiang 2014

Abstract

Legendre Moment has been applied in image reconstruction since early years. In this research, a numerical integration method is proposed to improve the computational accuracy of Legendre moments. To clarify the improved computation scheme, image reconstructions from higher orders of Legendre moments, up to 240, are conducted. With the more accurate generated moments, the distributions of image information in a finite set of Legendre moments is investigated. We have concluded that each individual finite set of Legendre moments will represent the unique image features independently, while the even orders of Legendre moments describe most of image characteristics.

Acknowledgements

The graduate study opportunity that I had with University of Winnipeg was a great experience for learning and developing professional research skills. I consider myself is a very lucky person that could be part of this research project. I am very grateful for having so many people and professionals who help and provide their valuable assistance in the preparation and completion of my entile graduate studies and research.

I am using this opportunity to express my special thanks to Dr. Simon Liao who provided all his valuable knowledge and guidance for my courses and research both theoretically and practically.

I also express my deepest thanks to my employer, WinnipegREALTORS®, and to my manager of the IT department, Mr. Dan Brooks, for creating an inspiring and friendly working environment and for supporting my graduate study by providing flexible working hours.

It is my pleasure to express my gratitude to the faculty of the Applied Computer Science department, for their support and administration.

Finally, I would like to thank my family, especially my husband, Norman

Tran, for his encouragement and support since I decided to pursue my next level of knowledge and skill. I thank my two lovely children, Naomi Tran and Jeremy Tran, who are also happy for my achievement and to my parents, who brought me to this wonderful world.

To accomplish this thesis is a big milestone in my life. I will strive to use all the skills and knowledge I learned in the best possible ways through out my career.

Contents

1 Introduction **1**

2 Moments Methods **4**

2.1 Introduction 4

2.2 Geometric Moments 6

2.3 Legendre Moments 9

3 Legendre Moments Computing **13**

3.1 Introduction 13

3.2 Computation of Legendre Moments 14

3.2.1 Approximation Error 14

3.2.2 Efficiency 15

3.3 Legendre Moments Calculation 17

4 Image Reconstruction from Legendre Moments **19**

4.1 Introduction 19

4.2 Image Reconstruction Theory 20

4.3 Error Measurement Methods 21
4.3.1 Mean Square Error (MSE) 21
4.3.2 Peak Signal to Noise Ratio (PSNR) 21
4.4 Image Reconstruction Computing 22
4.5 Image Reconstruction Results 24
4.5.1 Square Images 24
4.5.2 Rectangle Images 33
4.6 Summary 38

5 Image Reconstruction from a Partial Set of Legendre Moments 39

5.1 Introduction 39
5.2 Image Reconstruction with Different Band of Legendre Moments 40
5.3 Image Reconstruction with Different Sets of Legendre Moments 47
5.4 Summary 51

6 Conclusions and Future Study 52

6.1 Conclusions 52
6.2 Future Study 53

List of Figures

2.1 The moment projections 8

2.2 The plots for function $\{P_m(x)\}$, m=1 to 6 on interval [-1,1]. . 10

2.3 The plots of lower m, n values of two-dimensional $P_m(x)P_n(y)$ Legendre polynomials. (a)$P_2(x)P_2(y)$, (b)$P_4(x)P_4(y)$, (c)$P_8(x)P_8(y)$ and (d)$P_{10}(x)P_{10}(y)$ 11

2.4 The plots of higher m, n values of two-dimensional $P_m(x)P_n(y)$ Legendre polynomials. (a)$P_{100}(x)P_{100}(y)$, (b)$P_{150}(x)P_{150}(y)$, (c) $P_{200}(x)P_{200}(y)$ and (d) $P_{240}(x)P_{240}(y)$ 12

3.1 The distribution of $P_{100}(x)P_{100}(y)$ in four different corner pixels of a 256×256 image. (a)Left top corner (b)Right top corner (c) Left low corner (d)Right low corner 16

3.2 The Legendre Moment Matrix 18

4.1 Four testing images of 256×256 with 256 different gray levels. 24

4.2 Some reconstructed images from different Ledendre moments orders with various $k \times k$ numerical schemes on Figure 4.1 (a). 25

4.3 PSNRs of the reconstructed Figure 4.1 (a) with different Legendre moment orders and $k \times k$ numerical schemes. 26
4.4 Some reconstructed images from different Ledendre moments orders with the 11×11 numerical scheme on Figure 4.1 (b). . 27
4.5 PSNRs of the reconstructed Figure 4.1 (b) with different Legendre moment orders and $k \times k$ numerical schemes. 28
4.6 Some reconstructed images from different Ledendre moments orders with various $k \times k$ numerical schemes on Figure 4.1 (c). 29
4.7 PSNRs of the reconstructed Figure 4.1 (c) with different Legendre moment orders and $k \times k$ numerical schemes. 30
4.8 Some reconstructed images from different Ledendre moments orders with various $k \times k$ numerical schemes on Figure 4.1 (d). 31
4.9 PSNRs of the reconstructed Figure 4.1 (d) with different Legendre moment orders and $k \times k$ numerical schemes. 32
4.10 Two testing images with 256 different gray levels: (a) is sized 182×256 and (b) is sized 256×174. 33
4.11 Some reconstructed images from different Legendre moments orders with various $k \times k$ numerical schemes on Figure 4.10 (a). 34
4.12 PSNRs of the reconstructed Figure 4.10 (a) with different Legendre moment orders and $k \times k$ numerical schemes. 35
4.13 Some reconstructed images from different Ledendre moments orders with various $k \times k$ numerical schemes on Figure 4.10 (b). 36

4.14 PSNRs of the reconstructed Figure 4.10 (b) with different Legendre moment orders and $k \times k$ numerical schemes. 37

5.1 Sub-figures (a) to (f) are the reconstructed images of Figure 4.1 (a), with applying 11 x 11 numerical scheme, from Legendre moments of orders 0 to 40, 41 to 80, 81 to 120, 121 to 200, 0 to 200, and the direct addition operation of images (a) to (d). 41

5.2 Sub-figures (a) to (f) are the reconstructed images of Figure 4.1 (b), with applying 11×11 numerical scheme, from Legendre moments of orders 51, 52, 53, 54, 55, and 51 to 55. The gray levels of all image pixels are multiplied by 10. 42

5.3 Sub-figures (a) to (f) are the reconstructed images of Figure 4.1 (b), with applying 11×11 numerical scheme, from Legendre moments of orders 196, 197, 198, 199, 200, and 196 to 200, respectively. The gray levels of all image pixels are multiplied by 25. 43

5.4 Images reconstructed from (a) all even number orders 0 to 240, (b) all odd number orders from 1 to 239, and (c) all orders from 0 to 240. 44

5.5 Images reconstructed from different even orders of Legendre moments with the 11×11 numerical scheme on Figure 4.1 (b). 45

5.6 PSNRs of the reconstructed Figure 4.1 (b) displayed in Figure 4.4 and Figure 5.5. 46
5.7 A set of λ Values for m-n=0 when minimum order = 0 and maximum order = 40 48
5.8 A set of λ Values for n=0 when minimum order = 0 and maximum order = 40 49
5.9 Image reconstructed with 1×1 numerical scheme on Minimum order 0 and Maximum Order 40 by applying different set of λ Values on Figure 4.1 (b) followed by different m-n or n values. 50

List of Tables

3.1 Computing time of order 240 Legendre moments for an image sized at 256×256 with different $k \times k$ numerical schemes. . . 16

4.1 PSNRs of different $k \times k$ numerical schemes for reconstruction performances on Figure 4.1 (a) 26

4.2 PSNR values of the 11×11 numerical scheme for reconstruction performances on Figure 4.1 (b) 28

4.3 PSNRs of different $k \times k$ numerical schemes for reconstruction performances on Figure 4.1 (c) 30

4.4 PSNRs of different $k \times k$ numerical schemes for reconstruction performances on Figure 4.1 (d) 32

4.5 PSNRs of different $k \times k$ numerical schemes for reconstruction performances on Figure 4.10 (a) 35

4.6 PSNRs of different $k \times k$ numerical schemes for reconstruction performances on Figure 4.10 (b) 37

List of Symbols

Some of the most frequently used mathematical symbols are summarized.

$f(x, y)$	=	Digital image as target with 256 grey levels
$\hat{f}(x, y)$	=	Reconstruction of image $f(x, y)$
M_{pq}	=	Moments Sequence
Φ_{pq}	=	Moment Function with (p, q) order
λ_{mn}	=	Legendre moments of order (m, n)
$\hat{\lambda_{mn}}$	=	Approximate Legendre moments of order (m, n)
$\Psi_{pq}(x, y)$	=	Moment Weighting Kernel of order (p, q)
$P_m(x)$	=	Legendre Polynomial
M_{max}	=	The maximum value of order
M	=	The size of image width
N	=	The size of image height
k	=	The size of numerical integral matrix
m	=	The order when calculating the Legendre moments
n	=	The order when calculating the Legendre moments

Chapter 1

Introduction

In our daily life, we are surrounded with a huge amount of different kinds of information. Information relies on different media to be transferred, processed, and analyzed. The digital image is one type of media that plays a very important role in information transmission as a communication tool. A two-dimensional image represents a finite set of digital values called pixels. A common digital image contains information and features through the values of pixels and can be used in many different industrial areas such as medicine, social media networks and security environments. The interpretation of image information is significantly important. Therefore, the need for image processing and analysis methods has increased rapidly.

Since Hu introduced the concept of image moments in 1962[8], many new achievements in theory of moments have been presented. The image moments are particularly calculated values of the image intensities and rep-

resent different types of information and global geometrical features of the image. Hu proposed the 2-D Geometric moments of an image as a structured element called "moment invariants", and constructed these invariants with low order moments, while the information in higher orders of moments were not utilized.

In 1980, Teague[16] introduced the orthogonal moments and proposed Zernike moments and Legendre moments, which utilize the Zernike polynomials and Legendre polynomials as the kernel functions. Teaque provided a foundation of orthogonal moment methods as the solution to the shortcoming of Geometric moments. The inverse moment transforms of these two orthogonal moments determine how well an image can be reconstructed from a set of moments.

Different types of conventional continuous orthogonal moments defined in a rectangular region have been investigated as the unique image shape features for applications in fields of pattern recognition and image analysis. As one of the important continuous orthogonal moments, the Legendre moment has been well investigated since the earlier years of moment-based descriptors studies[16][18][9]. However, some computational issues have bottlenecked the further development of efficient applications driven by Legendre moment-based techniques. The objective of this research is to study the image representing characteristics of Legendre moments and demonstrate their potential usefulness in the field of image analysis.

In this research, we have analyzed the computational errors and have

proposed an efficient method to improve the accuracy of Legendre moments computing, especially for the higher order moments. With the substantially improved accurate Legendre moments, the image reconstructions from Legendre moments, up to the order of 240, are performed with highly satisfactory results. We have also conducted the image reconstructions from a finite set and individual Legendre moments. This leads to the clarification that the lower order of Legendre moments mainly contain fundamental image information, while the higher order of Legendre moments preserve more detailed image information. We refer to books written by Mukundan and Ramakrishnan[11], Pawlak[13], and Flusser et al. [5] as background studies of moment methods for this research.

The organization of this thesis is as follows: Chapter 2 will overview the general concept of moments; Chapter 3 will review the general properties of Legendre moments and the computational errors in Legendre moment computing. In Chapter 4 will verify more accurate Legendre moment computational results and some reconstructed images from the higher orders of Legendre moments are represented. The investigation of representing characteristics of a partial set of Legendre moments in image analysis is performed in Chapter 5. Finally, the conclusions and suggested future studies are reported in Chapter 6.

Chapter 2

Moments Methods

2.1 Introduction

The concept of moments has been around for many years and widely applied in many scientific fields such as mechanics and statistics.

The methods of image moments were introduced by Hu[8] in 1962. His *Uniqueness Theorem* states that the moment sequence of an image function $f(x, y)$, $\{M_{pq}\}$, is defined by

$$M_{pq} = \int_{-\infty}^{+\infty} \int_{-\infty}^{+\infty} x^p \, y^q \, f(x, y) \, dxdy, \qquad p, q = 0, 1, 2, 3..., \tag{2.1}$$

is uniquely determined by $f(x, y)$; and conversely, $f(x, y)$ is uniquely determined by $\{M_{pq}\}$. It is assumed the image function $f(x, y)$ is piecewise continuous and can have nonzero values only in the finite part of the (x, y)

plane.

Hu[8] derived a set of seven invariant moments which contains the invariant properties under image translation, rotation, scaling, and skew. Since then, many new achievements in the theory of moments have been presented. Each moment method has its own specific functions to be advantageous on different applications. In 1980, Teague[16] introduced the orthogonal moments and proposed two important orthogonal moments, Zernike moments and Legendre moments, in image analysis as a solution to the inherent drawback of Geometric moments.

The general definition of the moment functions Φ_{pq} with $(p+q)$ order of the image function $f(x,y)$ is given by [11]:

$$\Phi_{pq} = \int_{-\infty}^{+\infty}\int_{-\infty}^{+\infty} \Psi_{pq}(x,y)\, f(x,y)\, dxdy, \qquad p,q = 0,1,2,3..., \tag{2.2}$$

where p, q are non-negative integers and $(p+q)$ is the order of moment Φ_{pq}. $\Psi_{pq}(x,y)$ is known as the moment weighting kernel, which consists the product of the polynomial basis function. For example, Zernike moments corresponds to Zernike polynomial function and Legendre moments corresponds to Legendre polynomial function.

This chapter provides an overview of some important moments and their properties.

2.2 Geometric Moments

The $(p+q)$th order of Geometric moments of an image function $f(x,y)$ are defined as[11]:

$$M_{pq} = \int_{-\infty}^{+\infty}\int_{-\infty}^{+\infty} x^p\, y^q\, f(x,y)\, dxdy, \qquad p,q = 0,1,2,3..., \tag{2.3}$$

where p,q = 0,1,2,3,...,∞, and x^py^q is the weighting kernel of this moment. Geometric moment is easily computed and implemented. As mentioned in the previous section, the *Uniqueness Theorem* states the fact that the values of moments can uniquely describe the information contained in image.

In general, the lower orders of Geometric moments represent the main fundamental characteristics of image intensity distribution. The zeroth-order moment, M_{00}, of the image function $f(x,y)$

$$M_{00} = \int_{a_1}^{a_2}\int_{b_1}^{b_2} f(x,y)\, dxdy, \tag{2.4}$$

represents the total mass of the image $f(x,y)$. For a digital image, the zeroth-order moment represents the total area of image region.

The first-order moments, M_{10} and M_{01}, defined as

$$M_{10} = \int_{a_1}^{a_2}\int_{b_1}^{b_2} x\, f(x,y)\, dxdy, \tag{2.5}$$

and

$$M_{01} = \int_{a_1}^{a_2} \int_{b_1}^{b_2} y\, f(x,y)\, dxdy, \tag{2.6}$$

describe the centre of mass of the image function $f(x, y)$. In term of moment values, the central coordinates (x_0, y_0) are

$$x_0 = \frac{M_{10}}{M_{00}} \tag{2.7}$$

$$y_0 = \frac{M_{01}}{M_{00}} \tag{2.8}$$

The second-order moment is known as moments of inertia[5] in mechanics. It can be used to determine the orientation of image function $f(x, y)$. Orientation usually describes the position and the direction of the image in the field of the view. If θ represents an orientation angle of the principal axis, it is defined by[7]:

$$\theta = \frac{1}{2}\, tan^{-1}\, (\frac{2\mu_{11}}{\mu_{20} - \mu_{02}}) \tag{2.9}$$

where θ is in the range of $[-\frac{\pi}{4}, \frac{\pi}{4}]$ and the μ_{11},μ_{20} and μ_{02} are the second-order central moments of an image in its actual image reference frame.

The image projection onto x and y axes is a special characteristic feature of moments that represents from a set of M_{p0} and M_{0q} moment values. Figure 2.1 shows the illustration of moments set projections. This concept will be further addressed in Chapter 5 by applying a partial set of Legendre moments with a maximum order of 240 on a digital image sized 256×256.

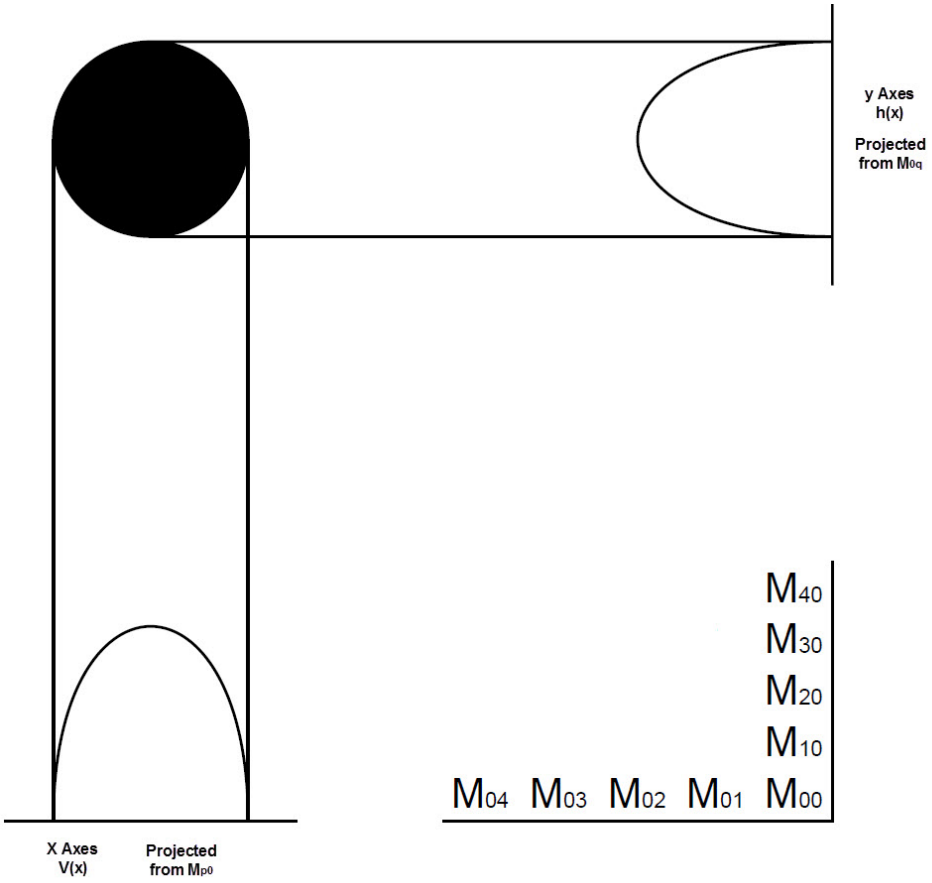

Figure 2.1: The moment projections

.

The lower orders of moments show the essential characteristics of an image function and the higher orders of moments represent more detailed image information.

2.3 Legendre Moments

The Legendre polynomial is the basis set for Legendre moment. The m-th order Legendre polynomial [14] is defined by the Rodrigues formula

$$P_m(x) = \frac{1}{2^m m!} \frac{d^m}{dx^m}(x^2 - 1)^m, \tag{2.10}$$

and its recurrent formula is

$$P_{m+1}(x) = \frac{2m+1}{m+1}\, x\, P_m(x) - \frac{m}{m+1}\, P_{m-1}(x). \tag{2.11}$$

The polynomial expressions for $\{P_m(x)\}$ up to sixth order are given below and Figure 2.2 represents their plots:

$$P_0(x) = 1 \tag{2.12}$$

$$P_1(x) = x \tag{2.13}$$

$$P_2(x) = \frac{3x^2 - 1}{2} \tag{2.14}$$

$$P_3(x) = \frac{5x^2 - 3x}{2} \tag{2.15}$$

$$P_4(x) = \frac{35x^4 - 30x^2 + 3}{8} \tag{2.16}$$

$$P_5(x) = \frac{63x^5 - 70x^3 + 15x}{8} \tag{2.17}$$

$$P_6(x) = \frac{231x^6 - 315x^4 + 105x^2 - 5}{16} \tag{2.18}$$

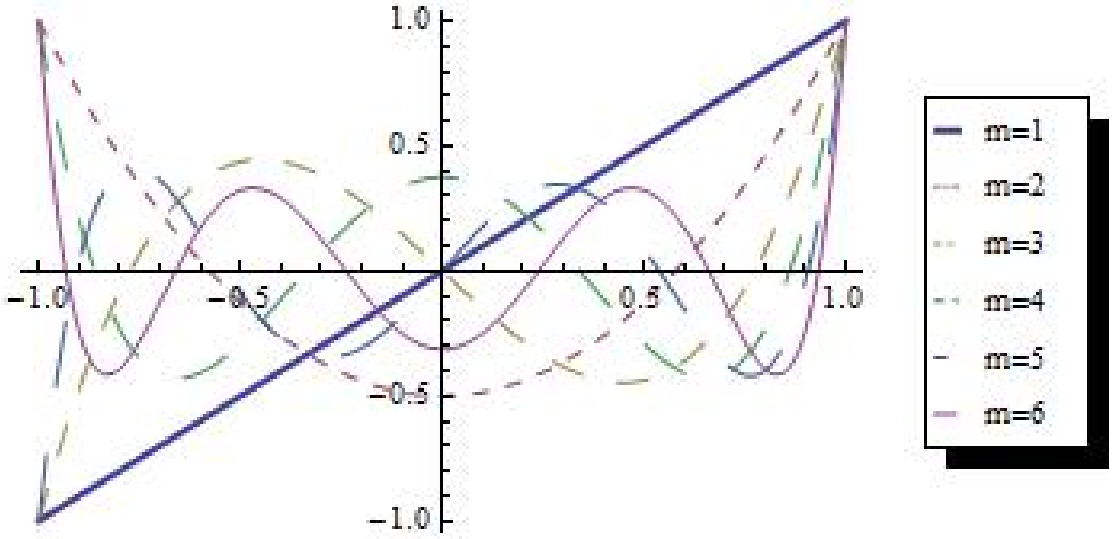

Figure 2.2: The plots for function $\{P_m(x)\}$, m=1 to 6 on interval [-1,1].

The Legendre polynomials $\{P_m(x)\}$[13] are a complete orthogonal basis set defined on the interval [-1, 1]

$$\int_{-1}^{+1} P_m(x)\, P_n(x) dx = \frac{2}{2n+1}\, \delta_{mn}, \tag{2.19}$$

where δ_{mn} is the Kronecker symbol.

The (m, n)-th order of Legendre moment of an image function $f(x, y)$ is defined on the square $[-1, 1] \times [-1, 1]$ by

$$\lambda_{mn} = \frac{(2m+1)(2n+1)}{4} \int_{-1}^{+1}\int_{-1}^{+1} f(x, y)\, P_m(x)\, P_n(y)\, dxdy, \tag{2.20}$$

where $m, n = 0, 1, 2, ...$

Figure 2.3 shows the distributions of some lower orders of $P_m(x)P_n(y)$ in

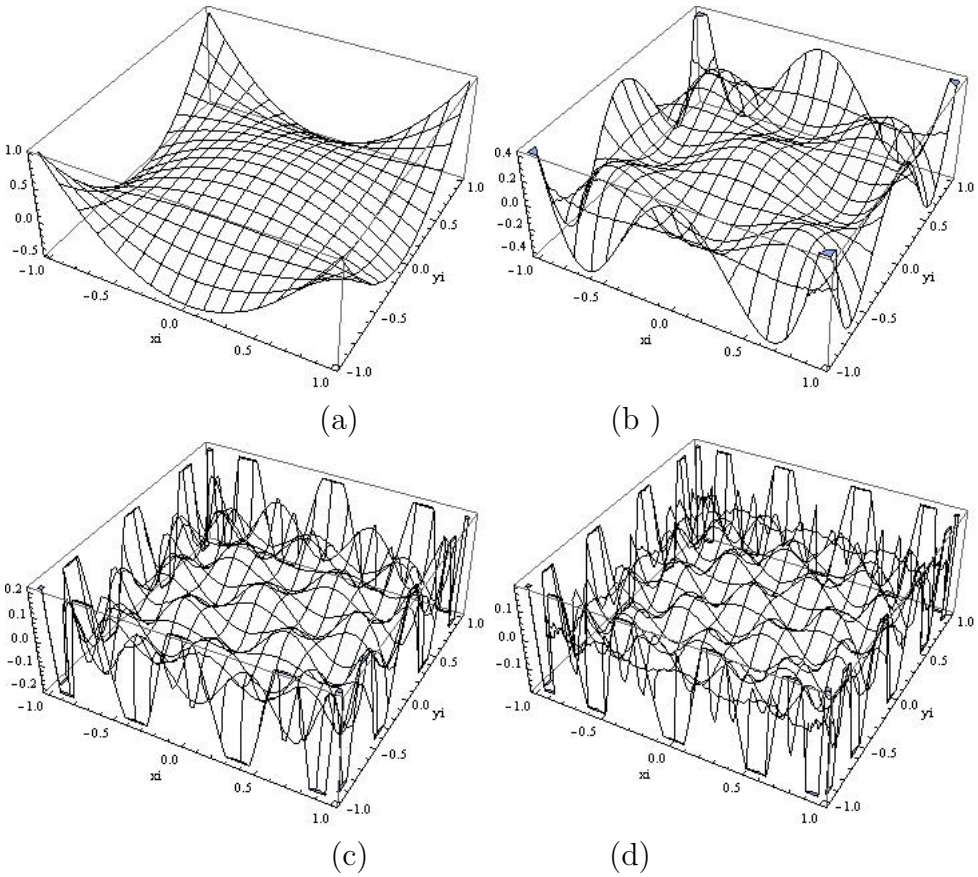

Figure 2.3: The plots of lower m, n values of two-dimensional $P_m(x)P_n(y)$ Legendre polynomials. (a)$P_2(x)P_2(y)$, (b)$P_4(x)P_4(y)$, (c)$P_8(x)P_8(y)$ and (d)$P_{10}(x)P_{10}(y)$

the region of $[-1, 1] \times [-1, 1]$, while Figure 2.4 represents the plots of higher orders of two-dimensional $P_m(x)P_n(y)$ Legendre polynomials.

In the case of digital image processing, the double integration in (2.20) needs to be replaced by double summations. Assuming a digital image is

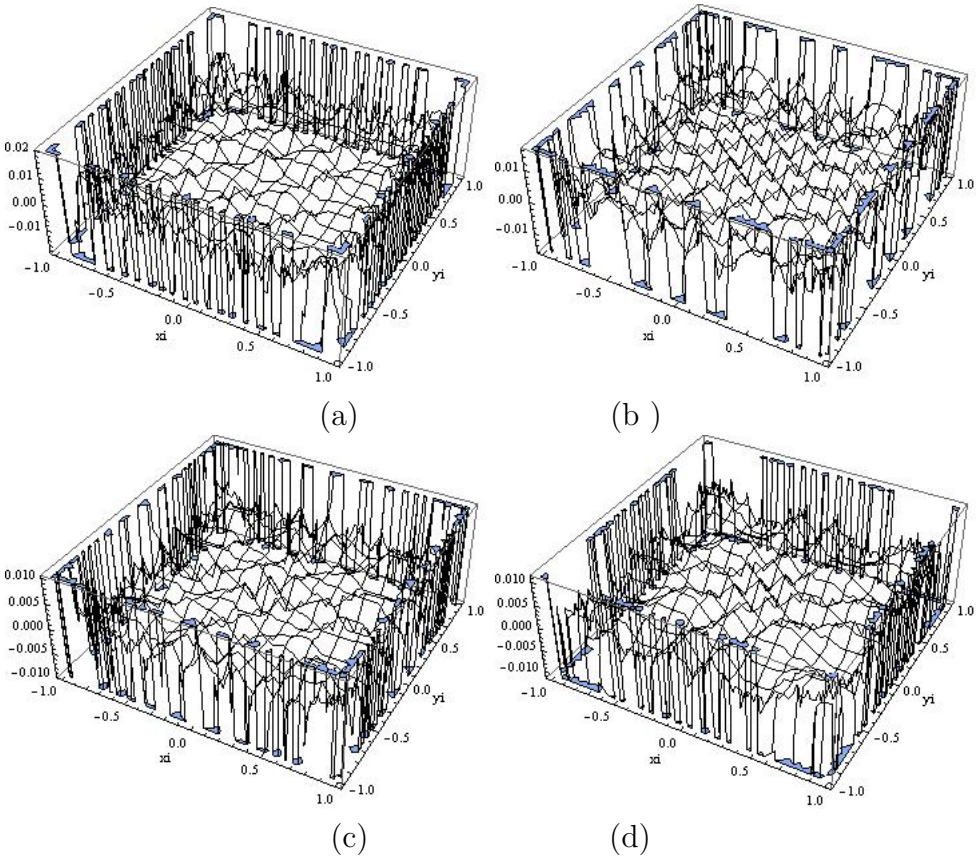

Figure 2.4: The plots of higher m, n values of two-dimensional $P_m(x)P_n(y)$ Legendre polynomials. (a)$P_{100}(x)P_{100}(y)$, (b)$P_{150}(x)P_{150}(y)$, (c) $P_{200}(x)P_{200}(y)$ and (d) $P_{240}(x)P_{240}(y)$

sized $M \times N$, (2.20) becomes

$$\lambda_{mn} = \frac{(2m+1)(2n+1)}{MN} \sum_{i=1}^{M} \sum_{j=1}^{N} f(x_i, y_j)\, P_m(x_i)\, P_n(y_j)\, \Delta x \Delta y, \qquad (2.21)$$

where $f(x_i, y_j)$ is the discrete version of $f(x, y)$. Δx and Δy are sampling intervals in the x and y directions.

Chapter 3

Legendre Moments Computing

3.1 Introduction

In digital image processing, we can only observe an image function $f(x, y)$ at discrete pixels, so the discrete version of $f(x, y)$ becomes $f(x_i, y_j)$. Therefore, the double integration in (2.20) need to be approximated by double summations. In Legendre moment computing, it has been a common practice to apply (2.21) directly. However, when the order of Legendre moments increases, $\Delta x \Delta y$ in (2.21) can no longer produce an accurate result.

3.2 Computation of Legendre Moments

3.2.1 Approximation Error

The (m, n)-th order of Legendre moment of an image function $f(x, y)$ is defined in (2.20)

$$\lambda_{mn} = \frac{(2m+1)(2n+1)}{4} \int_{-1}^{+1}\int_{-1}^{+1} f(x,y)\, P_m(x)\, P_n(y)\, dxdy, \tag{3.1}$$

where $m, n = 0, 1, 2, ...$, and the m-th order Legendre polynomial defined in (2.10) is[14]

$$P_m(x) = \frac{1}{2^m m!} \frac{d^m}{dx^m}(x^2 - 1)^m. \tag{3.2}$$

To improve the accuracy of Legendre moment computation, we approximate λ_{mn} by [1]

$$\widehat{\lambda}_{mn} = \sum_{i=1}^{M}\sum_{j=1}^{N} f(x_i, y_j)\, h_{mn}(x_i, y_j), \tag{3.3}$$

where

$$h_{mn}(x_i, y_j) = \int_{x_i-\frac{\Delta x}{2}}^{x_i+\frac{\Delta x}{2}} \int_{y_j-\frac{\Delta y}{2}}^{y_j+\frac{\Delta y}{2}} P_m(x)\, P_n(y)\, dxdy. \tag{3.4}$$

Considering that $P_m(x)$ and $P_n(y)$ are independent, (3.4) can be rewritten as

$$h_{mn}(x_i, y_j) = \int_{x_i-\frac{\Delta x}{2}}^{x_i+\frac{\Delta x}{2}} P_m(x)\, dx \int_{y_j-\frac{\Delta y}{2}}^{y_j+\frac{\Delta y}{2}} P_n(y)\, dy. \tag{3.5}$$

Figure 3.1 shows the distributions of Legendre polynomials in the corner

pixels of a 256×256 image. It is obvious that the integration of $P_{100}(x)P_{100}(y)$ within each of the corner pixels is different from $\Delta x \Delta y$. If only one point of a pixel value is used for the moment calculation, it will generate significant computational errors. By using some well-known techniques of numerical integration, the integrations in (3.4) can be approximated with various accuracies. For example, the alternative extended Simpson's rule was applied to compute Legendre moments[4][9]. In this research, however, a straightforward $k \times k$ numerical scheme is utilized to calculate the double integrations in (3.4) [19]. By dividing a pixel into $k \times k$ sub regions with the same weights, we can reduce the computation errors of Legendre polynomials substantially. How much errors were reduced by increasing $k \times k$ value can be evaluated by PSNR values. In Chapter 4 will show PSNR results of the different $k \times k$ numerical schemes for each testing image's reconstruction performances.

3.2.2 Efficiency

Although computer technology has improved extremely in recent years, the process of computing higher order moments is still very time consuming. In this research, a desktop computer with CPU of 3.40GHz and 8.0 GB RAM was used.

One of the important tasks in this research is to reduce the computing hours. To avoid duplicative Legendre polynomial calculating, we have stored the values of all Legendre polynomial in an array. Retrieving the Legendre polynomial values directly from the array to compute the Legendre moments

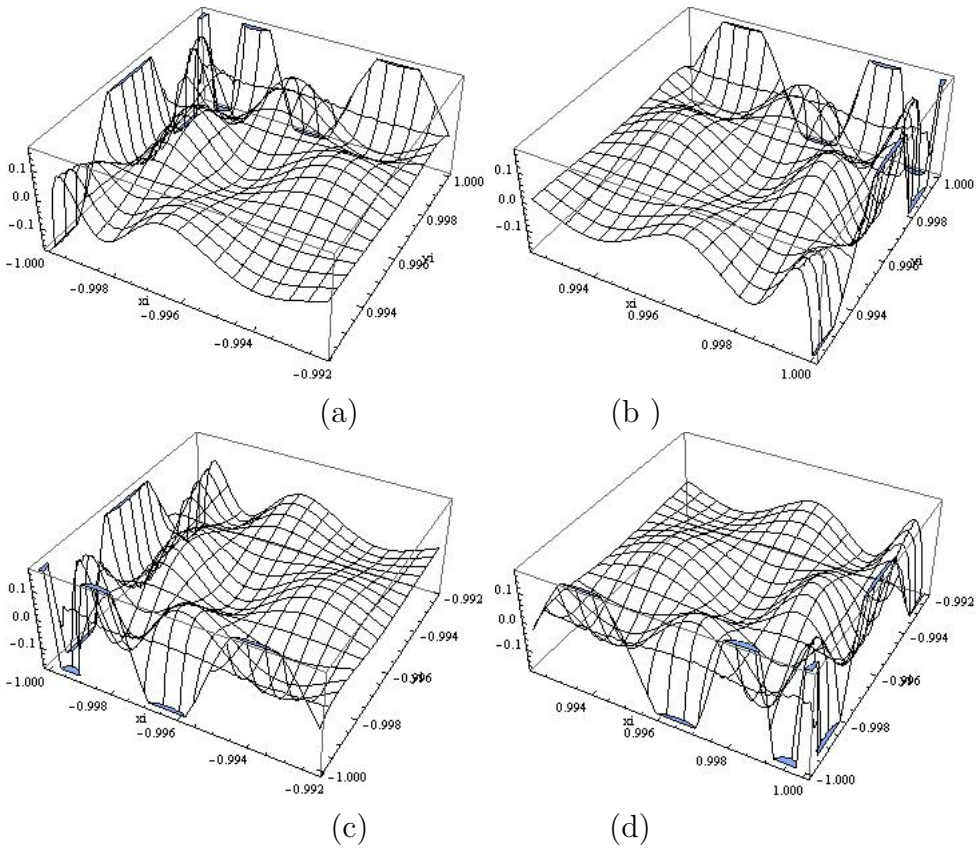

Figure 3.1: The distribution of $P_{100}(x)P_{100}(y)$ in four different corner pixels of a 256×256 image. (a)Left top corner (b)Right top corner (c) Left low corner (d)Right low corner

has significantly increased the efficiency of the computational procedure.

For an image sized at 256×256, Table 3.1 shows the computing time of Legendre moments of order 240 with different $k \times k$ numerical schemes.

Table 3.1: Computing time of order 240 Legendre moments for an image sized at 256×256 with different $k \times k$ numerical schemes.

Order(M_{max})	Hours
1×1	5.150
3×3	16.597
5×5	38.829
7×7	71.597
9×9	115.540
11×11	170.910

3.3 Legendre Moments Calculation

Algorithm 1
Legendre Polynomial
$MaxOrder$ = The Maximum order of Legendre Moments
to be calculated
$SizeH$ = Image Height in Pixels
$SizeW$ = Image Width in Pixels
k = Numerical number of points on each side of pixel
$Const = ((2 * m) + 1) * ((2 * n) + 1))/(SizeH * SizeW)$
$delta = 2/256$
Compute Legendre Polynomial Values for each Δx and Δy
$T(x)$ = Legendre polynomial array for Δx
$T(y)$ = Legendre polynomial array for Δy
For $m = 0$ to $MaxOrder$
For $i = 1$ to $Size$
For $h = 1$ to k
$x_i = (-1) + ((i - 1) * delta) + (delta/2 * k) + ((h - 1) * (delta/k))$
$y_i = (1) - ((i - 1) * delta) - (delta/2 * k) - ((h - 1) * (delta/k))$
$T(x) = LegendreP(m, x_i)$
$T(y) = LegendreP(m, y_i)$
End
End
End

Compute Legendre Moments of the image
TM = A table to store moments for a image
For $m = 0$ to $MaxOrder$
For $n = 0$ to $MaxOrder - m$
$h_{mn} = (\sum\sum P_{m,x}\ P_{n,y})\ /(k * k)$
$\lambda_{mn} = \sum\sum h_{mn}\ f(x, y)$
$TM = \lambda_{mn}$ * $Const$
End
End

$$\begin{pmatrix} \lambda_{0,0} & 0 & 0 & \cdots & 0 \\ \lambda_{1,0} & \lambda_{0,1} & 0 & \cdots & 0 \\ \lambda_{2,0} & \lambda_{1,1} & \lambda_{0,2} & \cdots & 0 \\ \vdots & \vdots & \vdots & \ddots & \vdots \\ \lambda_{m,0} & \lambda_{m-1,1} & \lambda_{m-2,2} & \cdots & \lambda_{0,m} \end{pmatrix}$$

Figure 3.2: The Legendre Moment Matrix

Algorithm 1 shows the algorithm to compute Legendre methods in this research and Legendre moments are produced in a matrix shown in Figure 3.2. For effective calculation time, the moment values were stored in a flat text file for image reconstruction computing. In this research, two different types of images were used, square and rectangle.

Chapter 4

Image Reconstruction from Legendre Moments

4.1 Introduction

To verify our proposed solutions for more accurate Legendre moment computation, we examine the image reconstruction determined by

$$\widehat{f}_{M_{max}}(x,y) = \sum_{m=0}^{M_{max}} \sum_{n=0}^{m} \widehat{\lambda}_{m-n,n}\, P_{m-n}(x)\, P_n(y), \tag{4.1}$$

with the Legendre moments $\lambda_{m-n,n}$ replaced by their approximations given by (3.3). It is important to note that when the given highest Legendre moment order M_{max} is increased, the previously determined $\widehat{\lambda}_{m-n,n}$ does not change. The verification is presented in the following sections.

4.2 Image Reconstruction Theory

As stated in Chapter 2, the Legendre polynomials $\{P_m(x)\}$[13] are a complete orthogonal basis set defined on the interval [-1, 1]

$$\int_{-1}^{+1} P_m(x)\, P_n(x) dx = \frac{2}{2n+1}\, \delta_{mn}, \tag{4.2}$$

where δ_{mn} is the Kronecker symbol.

According to the orthogonality property of the Legendre moments, we can reconstruct an original image from an infinite series of its Legendre moments by

$$f(x,y) = \sum_{m=0}^{\infty} \sum_{n=0}^{m} \lambda_{m-n,n}\, P_{m-n}(x)\, P_n(y), \tag{4.3}$$

where the $(m,n)-th$ order of Legendre moment of an image function $f(x,y)$ is defined in (2.20)

$$\lambda_{mn} = \frac{(2m+1)(2n+1)}{4} \int_{-1}^{+1}\int_{-1}^{+1} f(x,y)\, P_m(x)\, P_n(y)\, dxdy.$$

In practice, however, we have to truncate the infinite series expressed in (4.3). If only Legendre moments of order $\leq M_{max}$ are given, the original image function $f(x,y)$ can be approximated by the truncated series

$$f(x,y) \simeq f_{M_{max}}(x,y) = \sum_{m=0}^{M_{max}} \sum_{n=0}^{m} \lambda_{m-n,n}\, P_{m-n}(x)\, P_n(y). \tag{4.4}$$

4.3 Error Measurement Methods

Mean Square Error (MSE) and Peak Signal to Noise Ratio (PSNR) methods are often used as measurements to compare two images in image processing.

4.3.1 Mean Square Error (MSE)

In statistics, Mean Square Error (MSE) is used to determine the difference between the estimator and what is estimated. Being applied in image processing, MSE is defined as[6]

$$MSE = \frac{1}{MN} \sum_{i=1}^{M} \sum_{j=1}^{N} [f(x_i, y_j) - \widehat{f}(x_i, y_j)]^2, \tag{4.5}$$

where $M \times N$ is the size of image, and $f(x, y)$ and $\widehat{f}(x_i, y_j)$ are the original and restored estimated images, respectively. The lower MSE value indicates the higher quality of restored image.

4.3.2 Peak Signal to Noise Ratio (PSNR)

Peak Signal to Noise Ratio(PSNR) is the ratio between the maximum power of the signal and the affecting noise, and is defined as

$$PSNR = 10 \log_{10}(\frac{G_{Max}^2}{MSE}) \tag{4.6}$$

where G_{Max} is the maximum gray level of the image, which is 255 in our case, and MSE is the Mean Square Error defined in (4.5).

To compare the reconstructed images with the original testing image, we have adopted the Peak Signal to Noise Ratio (PSNR) as the measurement, which is image independent and can be used to evaluate the reconstruction performance generally. The higher PSNR value indicates the higher quality of a restored image.

4.4 Image Reconstruction Computing

According to (4.4), an image can be approximated reconstructed by

$$f_{M_{max}}(x,y) = \sum_{m=0}^{M_{max}} \sum_{n=0}^{m} \lambda_{m-n,n}\, P_{m-n}(x)\, P_n(y), \tag{4.7}$$

where $\lambda_{m-n,n}$ is retrieved from Legendre Moment Matrix. Algorithm 2 shows how to perform the image reconstruction from Legendre moments.

Algorithm 2
Reconstruction using Legendre Moments
$MaxOrder$ = The Maximum order of Legendre Moments
to be calculated
$sizeW$ = The width of Image in Pixels
$sizeH$ = The height of Image in Pixels
k = Numerical number of points on each side of pixel
$ReImg$ = Table to store restored image data
$size$ = Image size

Compute Legendre Polynomial Values for each Δx and Δy
$T(x)$ = Legendre polynomial array for Δx
$T(y)$ = Legendre polynomial array for Δy
$deltax = 2/size$

For $m = 0$ to $MaxOrder$
For $j = 1$ to $sizeW$
$xi = (-1) + (deltax/2) + ((i-1) * deltax)$
$T(x) = LegendreP(m, x_i)$
End
End
For $m = 0$ to $MaxOrder$
For $i = 1$ to $sizeH$
$yi = (-1) + (deltax/2) + ((i-1) * deltax)$
$T(y) = LegendreP(m, y_i)$
End
End

Compute Reconstruction for an Image
TM = A table to store restored image data
For $i = 1$ to $sizeW$
For $j = 1$ to $sizeH$
$TM = \sum_{m=0}^{M_{max}} \sum_{n=0}^{m} \lambda_{m-n,n} \, P_{m-n}(x) \, P_n(y)$
End
End

4.5 Image Reconstruction Results

4.5.1 Square Images

Figure 4.1 shows four testing images utilized in this research. All images are sized 256×256 with 256 different gray levels. The four testing images represent different levels of information detail within each image.

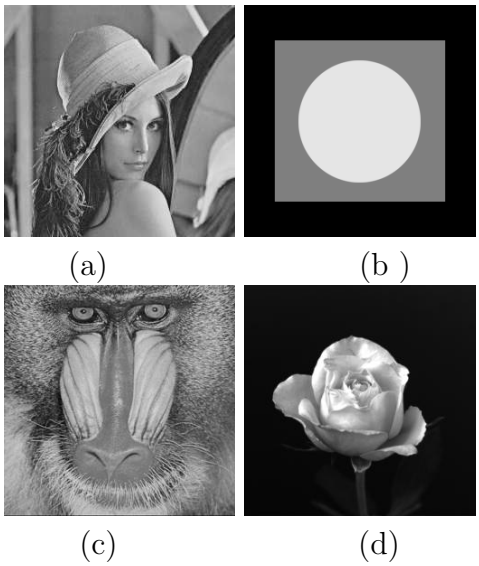

(a) (b) (c) (d)

Figure 4.1: Four testing images of 256×256 with 256 different gray levels.

We have conducted the image reconstructions from different maximum Legendre moment orders with various $k \times k$ numerical schemes. Figure 4.3 shows the plotting of PSNR values from the Legendre moment reconstruction performances on testing image Figure 4.1 (a) with different maximum orders and $k \times k$ numerical schemes, while Table 4.1 displays some values presented in Figure 4.3.

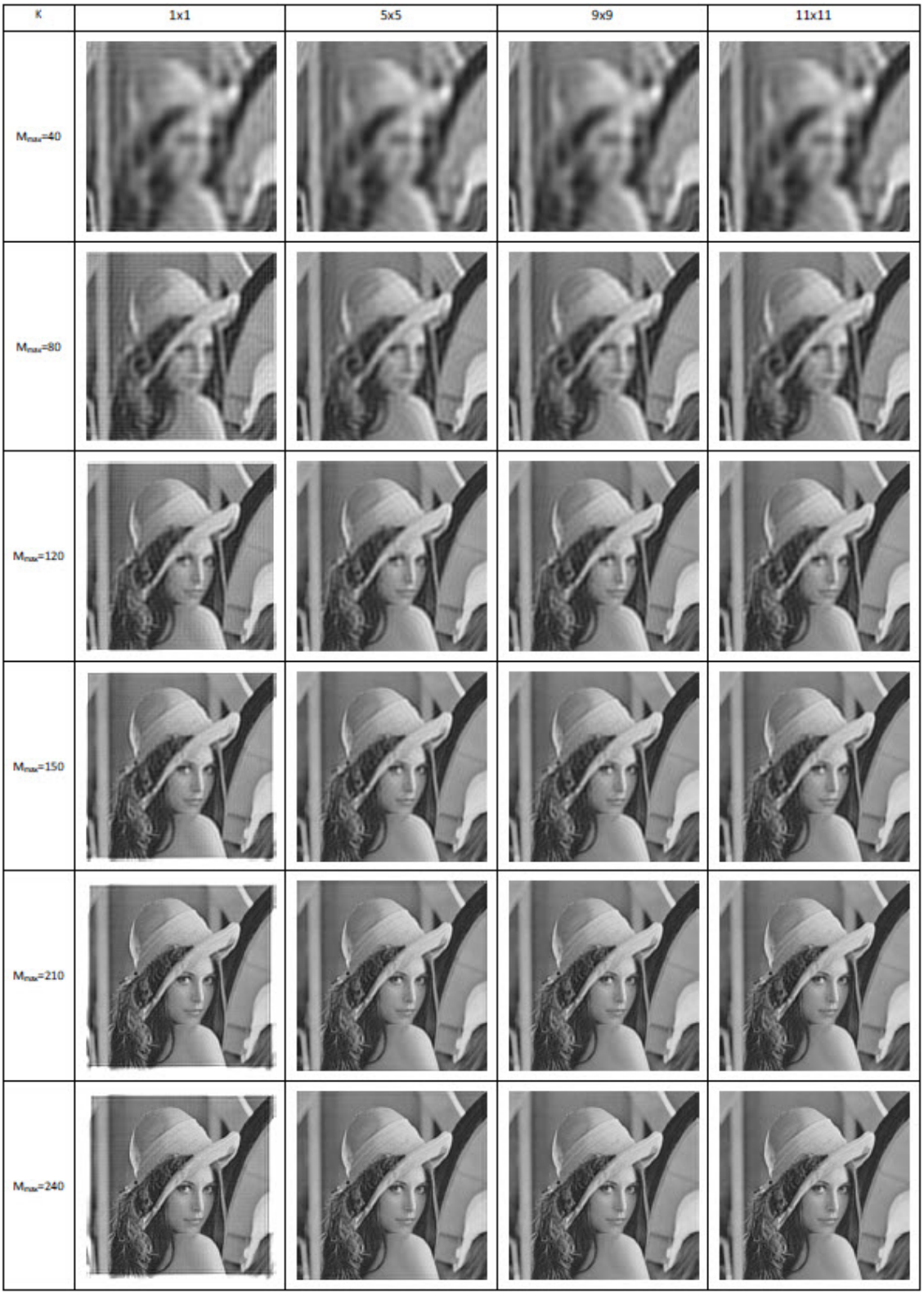

Figure 4.2: Some reconstructed images from different Ledendre moments orders with various $k \times k$ numerical schemes on Figure 4.1 (a).

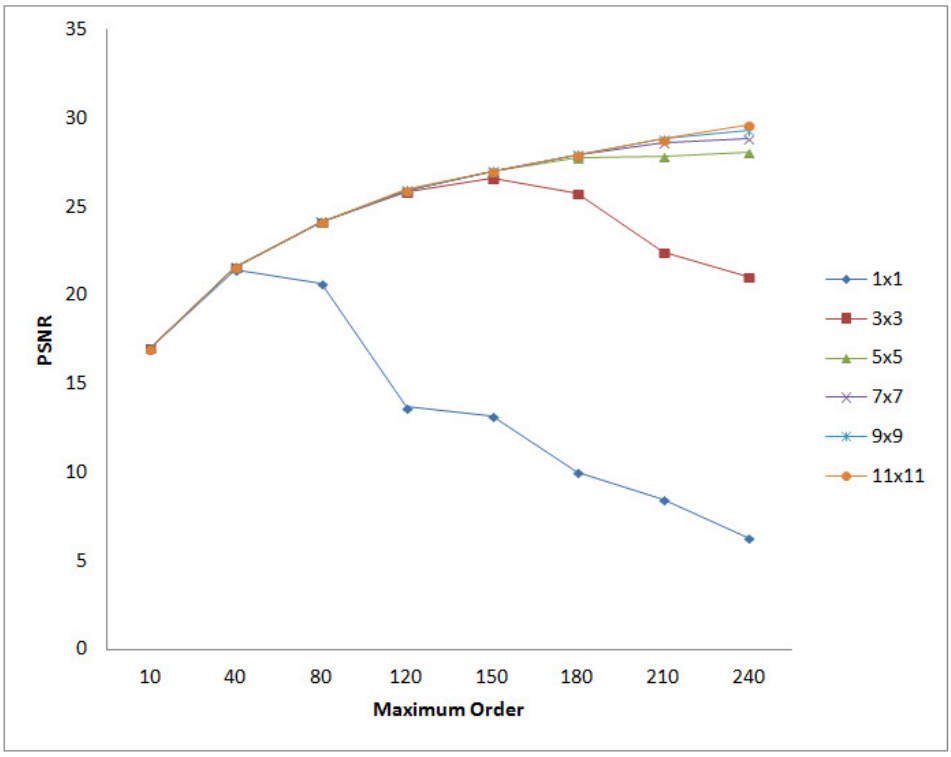

Figure 4.3: PSNRs of the reconstructed Figure 4.1 (a) with different Legendre moment orders and $k \times k$ numerical schemes.

Table 4.1: PSNRs of different $k \times k$ numerical schemes for reconstruction performances on Figure 4.1 (a)

Order(M_{max})	10	40	80	120	150	180	210	240
1×1	16.987	21.460	20.681	13.676	13.184	9.994	8.455	6.331
3×3	16.987	21.591	24.098	25.798	26.575	25.748	22.438	21.042
5×5	16.987	21.593	24.144	25.902	26.961	27.743	27.845	28.055
7×7	16.987	21.593	24.154	25.922	27.006	27.934	28.609	28.833
9×9	16.987	21.593	24.156	25.942	27.008	27.927	28.839	29.283
11×11	16.987	21.593	24.157	25.952	27.013	27.931	28.822	29.637

Table 4.2 shows some selected PSNR values from image reconstruction performances on testing image Figure 4.1 (b) with the 11×11 numerical scheme and different maximum Legendre moment orders.

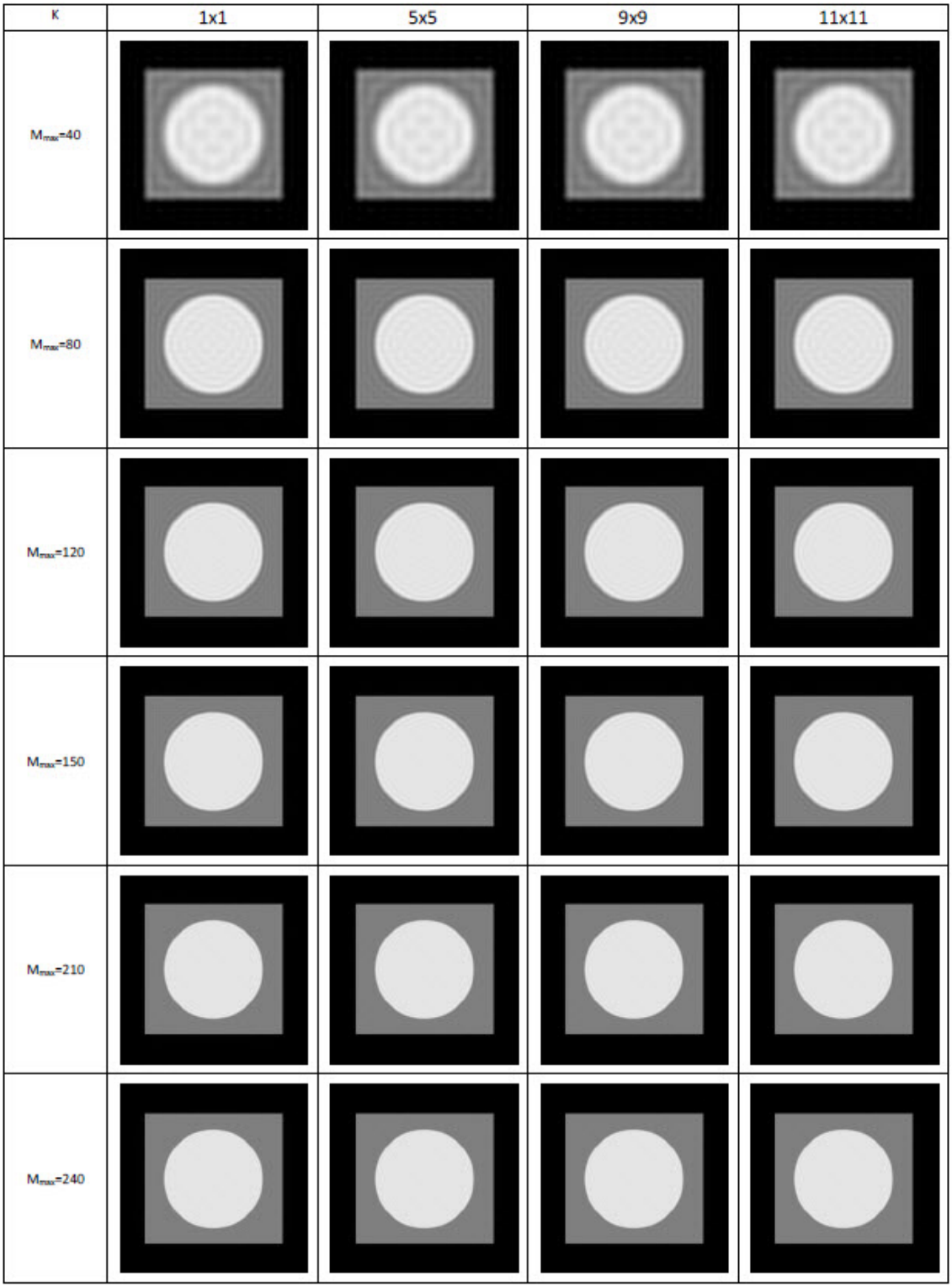

Figure 4.4: Some reconstructed images from different Ledendre moments orders with the 11×11 numerical scheme on Figure 4.1 (b).

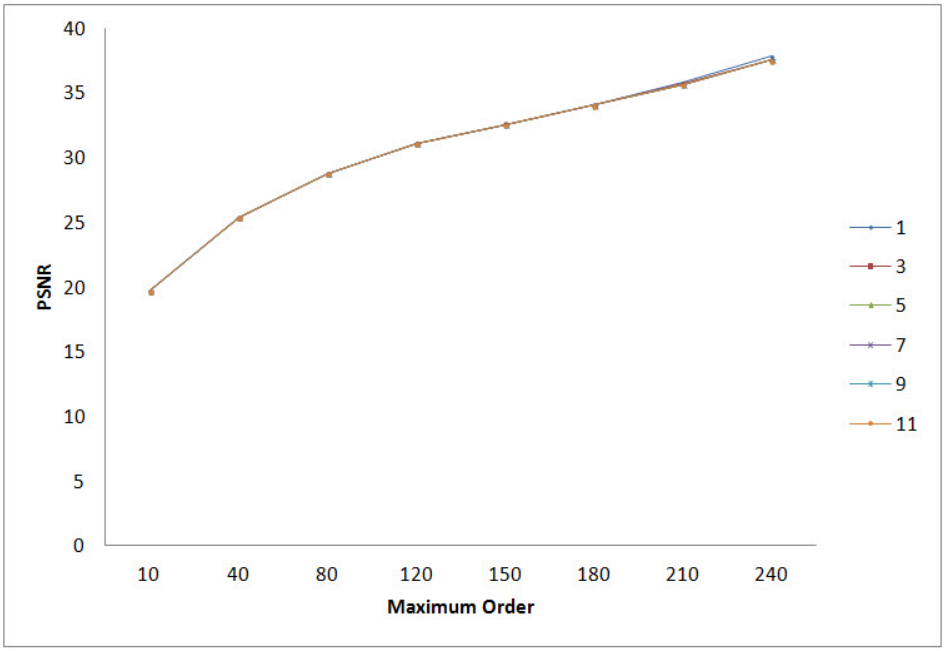

Figure 4.5: PSNRs of the reconstructed Figure 4.1 (b) with different Legendre moment orders and $k \times k$ numerical schemes.

Table 4.2: PSNR values of the 11×11 numerical scheme for reconstruction performances on Figure 4.1 (b)

Order(M_{max})	10	40	80	120	150	180	210	240
1×1	19.641	25.384	28.760	31.103	32.577	34.096	35.794	37.871
3×3	19.641	25.384	28.759	31.097	32.599	34.048	35.676	37.588
5×5	19.641	25.384	28.759	31.096	32.556	34.041	35.658	37.548
7×7	19.641	25.384	28.759	31.096	32.556	34.039	35.654	37.537
9×9	19.641	25.384	28.759	31.095	32.555	34.038	35.652	37.532
11×11	19.641	25.384	28.759	31.095	32.555	34.037	35.651	37.530

Figure 4.2 demonstrates some images reconstructed from Figure 4.1 (a) with various $k \times k$ numerical schemes and different maximum Legendre moment orders. It can be observed that the images reconstructed from higher

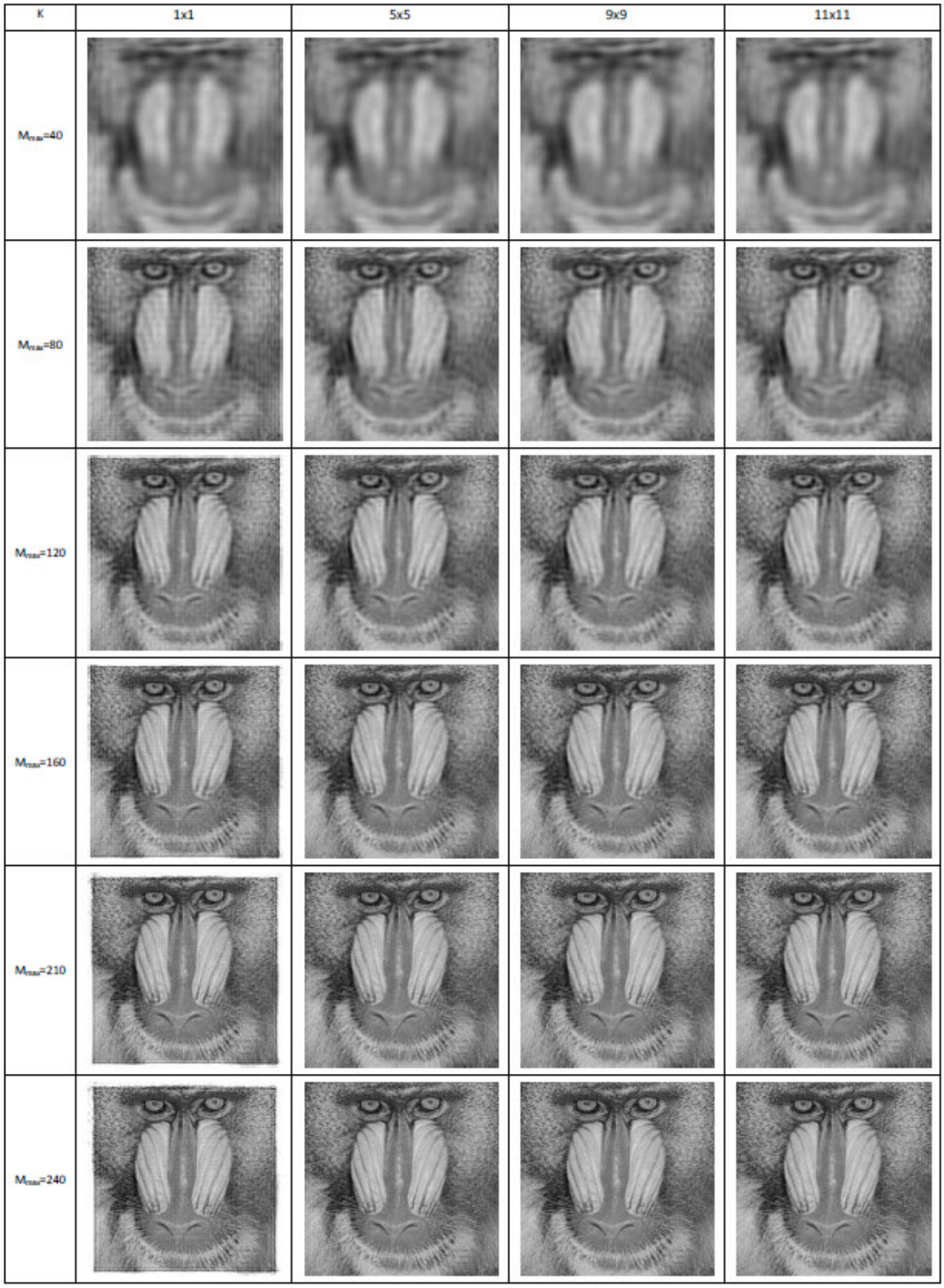

Figure 4.6: Some reconstructed images from different Ledendre moments orders with various $k \times k$ numerical schemes on Figure 4.1 (c).

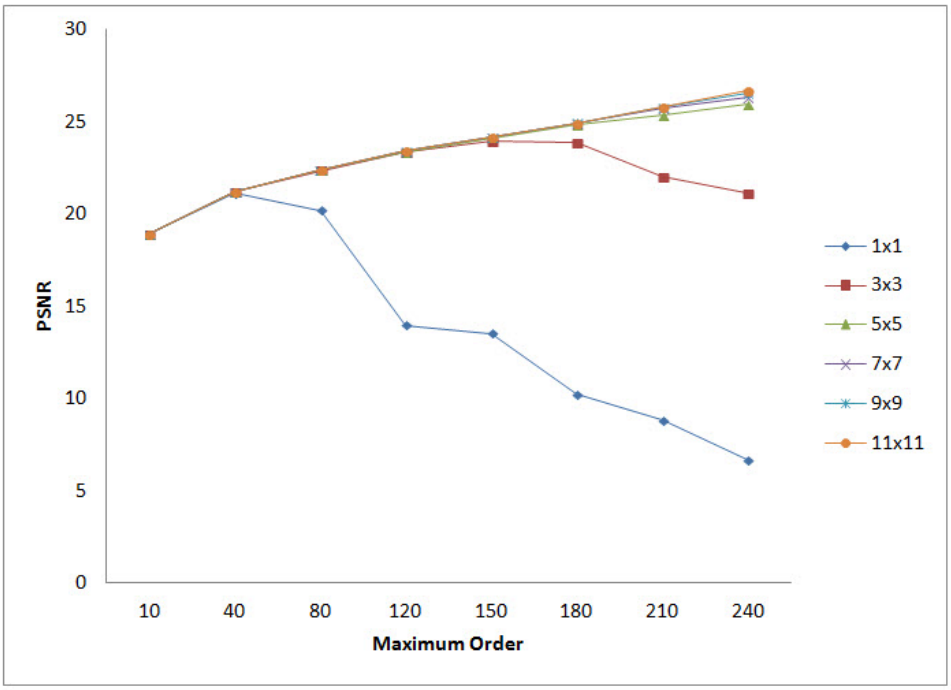

Figure 4.7: PSNRs of the reconstructed Figure 4.1 (c) with different Legendre moment orders and $k \times k$ numerical schemes.

Table 4.3: PSNRs of different $k \times k$ numerical schemes for reconstruction performances on Figure 4.1 (c)

Order(M_{max})	10	40	80	120	150	180	210	240
1×1	16.360	21.069	22.503	17.542	17.394	13.875	12.914	10.818
3×3	16.355	21.105	24.951	27.463	28.639	28.565	26.346	25.113
5×5	16.355	21.100	24.982	27.498	28.920	29.996	30.614	30.994
7×7	16.355	21.099	24.984	27.523	28.838	30.341	31.099	31.958
9×9	16.355	21.098	24.984	27.544	28.843	30.346	31.484	32.344
11×11	16.355	21.097	24.983	27.555	28.867	30.345	31.540	32.653

orders of Legendre moments with 7×7 and 11×11 numerical schemes appear to be very close to the original Figure 4.1 (a).

Figure 4.4 presents some reconstructed images from Figure 4.1 (b) with

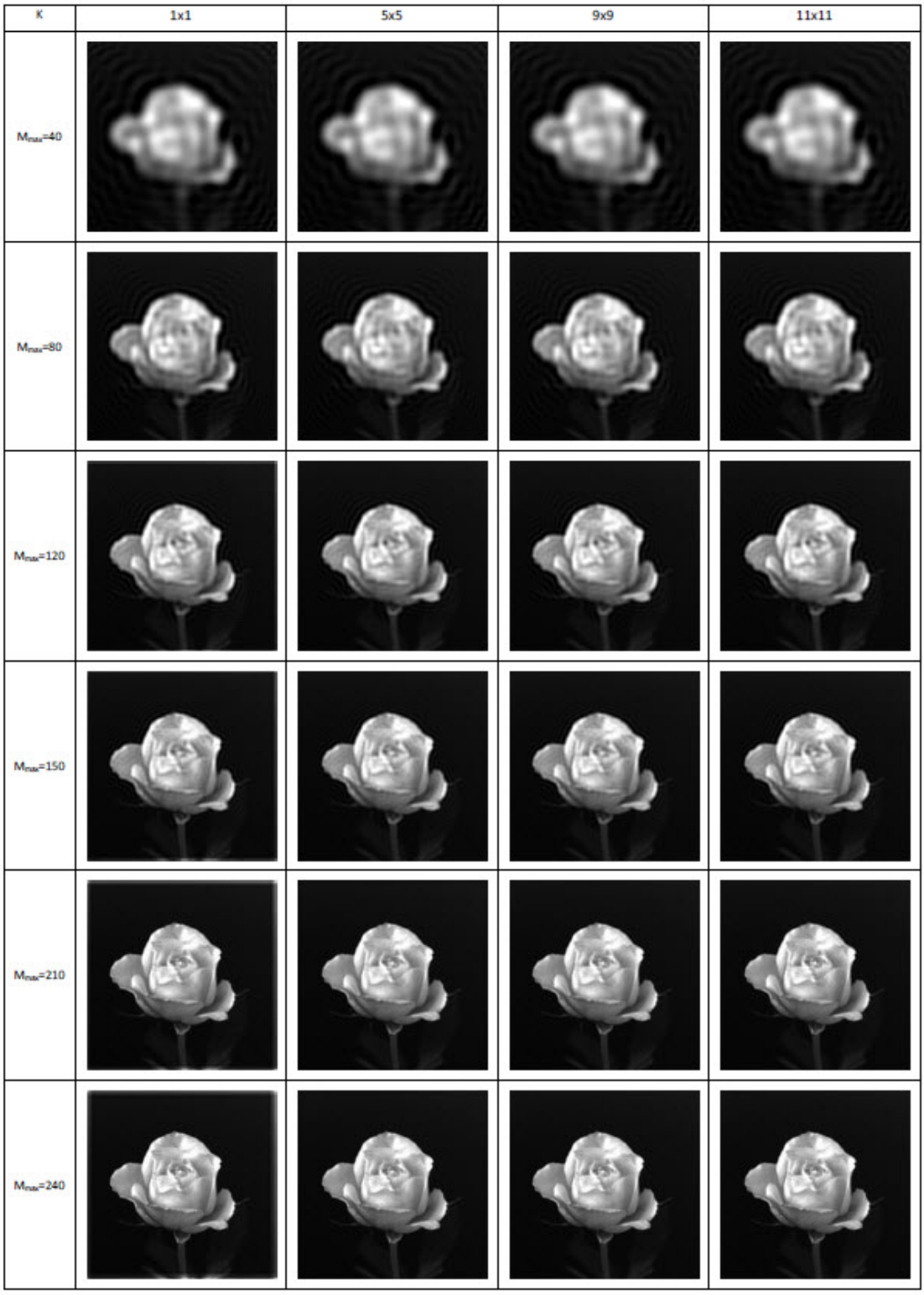

Figure 4.8: Some reconstructed images from different Ledendre moments orders with various $k \times k$ numerical schemes on Figure 4.1 (d).

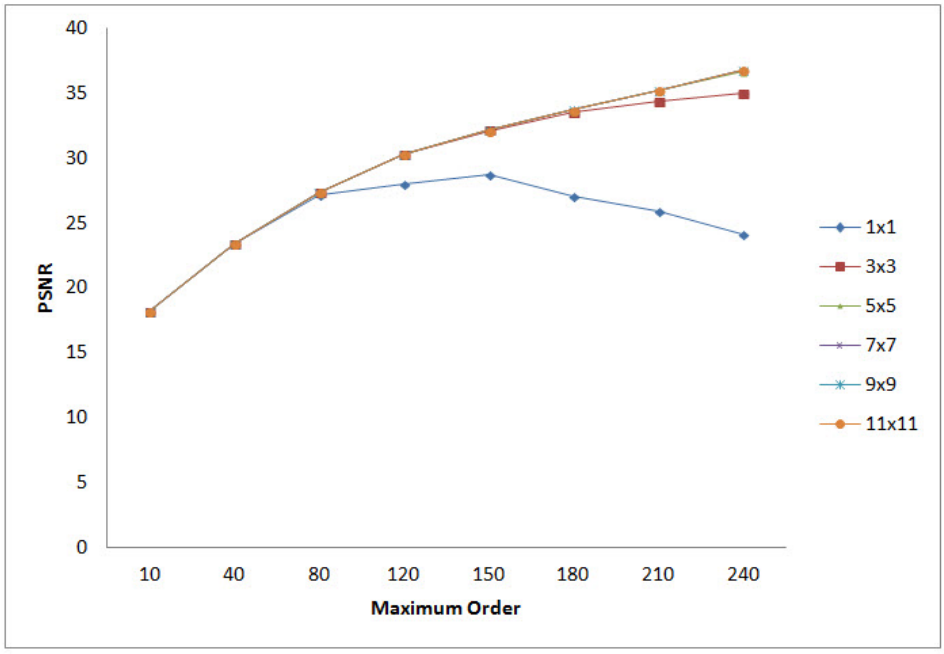

Figure 4.9: PSNRs of the reconstructed Figure 4.1 (d) with different Legendre moment orders and $k \times k$ numerical schemes.

Table 4.4: PSNRs of different $k \times k$ numerical schemes for reconstruction performances on Figure 4.1 (d)

Order(M_{max})	10	40	80	120	150	180	210	240
1×1	18.184	23.418	27.188	28.025	28.717	27.039	25.945	24.106
3×3	18.184	23.421	27.370	30.293	32.114	33.560	34.333	34.981
5×5	18.184	23.421	27.371	30.298	32.135	33.716	35.181	36.668
7×7	18.184	23.421	27.371	30.298	32.137	33.726	35.241	36.751
9×9	18.184	23.421	27.371	30.299	32.137	33.725	35.257	36.794
11×11	18.184	23.421	27.371	30.300	32.137	33.725	35.255	36.824

the 11×11 numerical scheme and different maximum Legendre moment orders.

4.5.2 Rectangle Images

To prove the same algorithm for square image should apply to non-square image like rectangle image, we selected two types of rectangle images with different image size of $M \times N$ as showing in Figure 4.10. Figure 4.10 (a) is sized 88×256 and Figure 4.10 (b) is sized 256×174. Both images have 256 different gray levels. The PSNR result for Figure 4.10 (a) and (b) are shown in Figure 4.12, 4.14 and Table 4.5, 4.6.

(a) (b)

Figure 4.10: Two testing images with 256 different gray levels: (a) is sized 182×256 and (b) is sized 256×174.

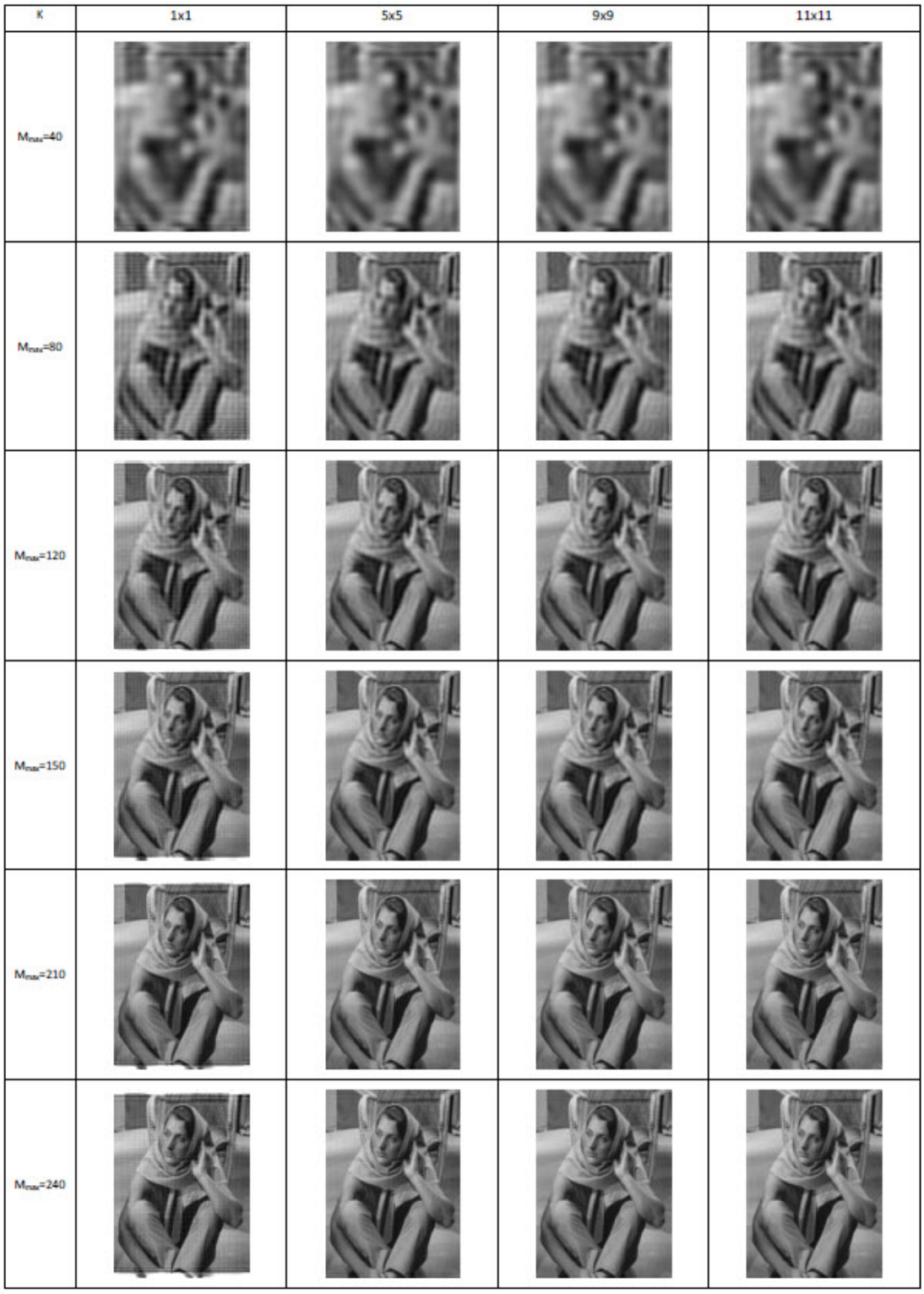

Figure 4.11: Some reconstructed images from different Legendre moments orders with various $k \times k$ numerical schemes on Figure 4.10 (a).

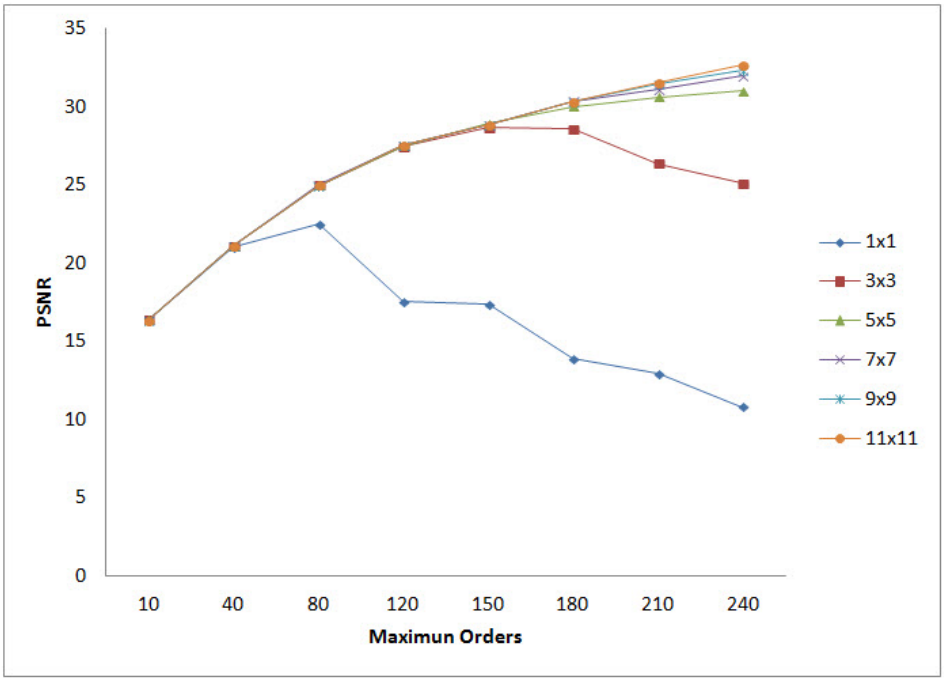

Figure 4.12: PSNRs of the reconstructed Figure 4.10 (a) with different Legendre moment orders and $k \times k$ numerical schemes.

Table 4.5: PSNRs of different $k \times k$ numerical schemes for reconstruction performances on Figure 4.10 (a)

Order(M_{max})	10	40	80	120	150	180	210	240
1×1	16.360	21.069	22.503	17.542	17.394	13.875	12.914	10.818
3×3	16.355	21.105	24.951	27.463	28.639	28.565	26.346	25.113
5×5	16.355	21.100	24.982	27.498	28.920	29.996	30.614	30.994
7×7	16.355	21.099	24.984	27.523	28.838	30.341	31.099	31.958
9×9	16.355	21.098	24.984	27.544	28.843	30.346	31.484	32.344
11×11	16.355	21.097	24.983	27.555	28.867	30.345	31.540	32.653

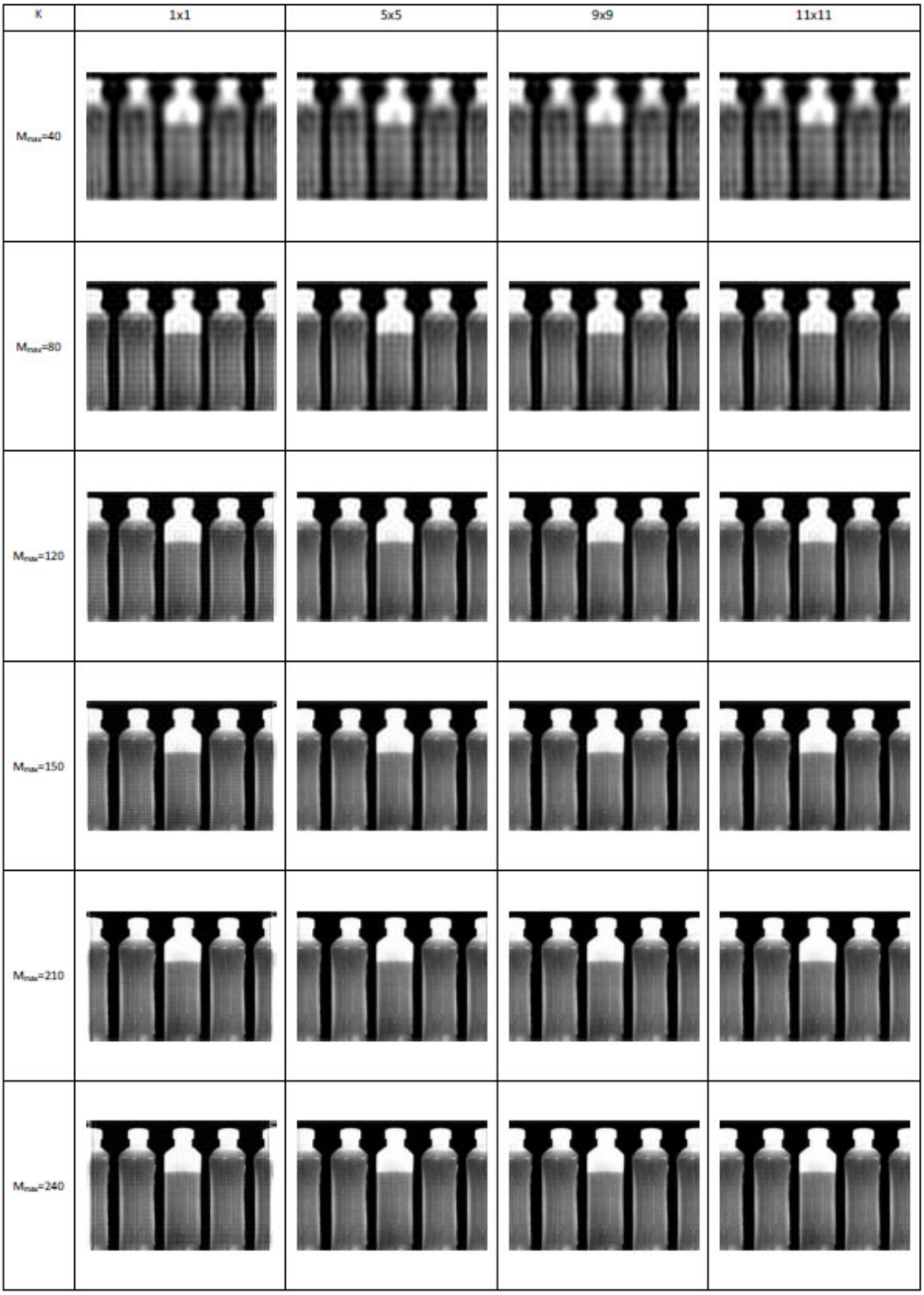

Figure 4.13: Some reconstructed images from different Ledendre moments orders with various $k \times k$ numerical schemes on Figure 4.10 (b).

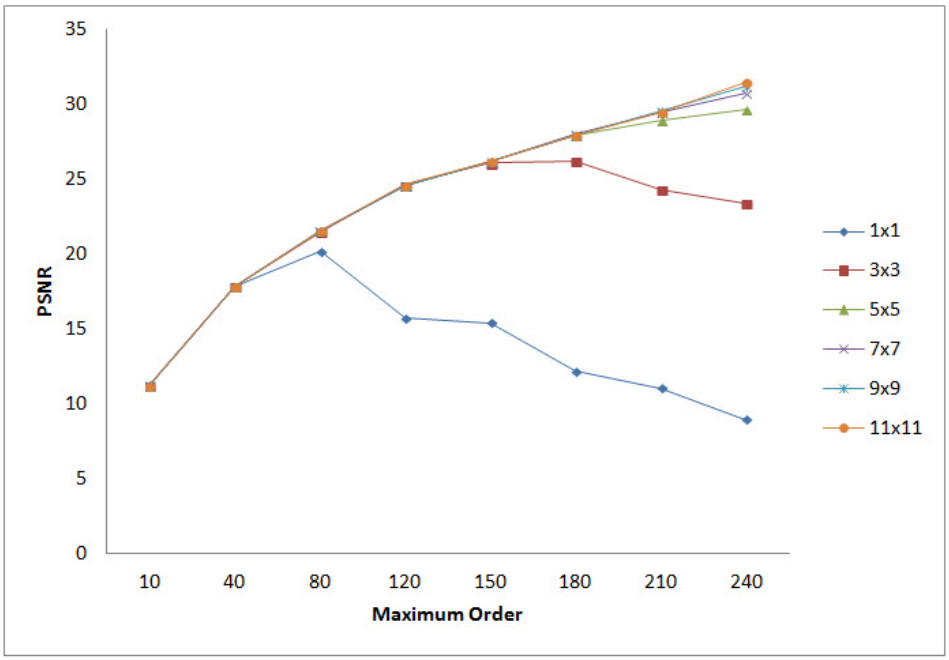

Figure 4.14: PSNRs of the reconstructed Figure 4.10 (b) with different Legendre moment orders and $k \times k$ numerical schemes.

Table 4.6: PSNRs of different $k \times k$ numerical schemes for reconstruction performances on Figure 4.10 (b)

Order(M_{max})	10	40	80	120	150	180	210	240
1×1	11.240	17.838	20.161	15.706	15.423	12.175	11.029	8.956
3×3	11.237	17.840	21.518	24.615	26.083	26.246	24.317	23.423
5×5	11.237	17.836	21.569	24.531	26.228	27.973	28.902	29.661
7×7	11.237	17.835	21.585	24.565	26.166	27.991	29.461	30.775
9×9	11.237	17.834	21.591	24.597	26.169	27.914	29.547	31.204
11×11	11.237	17.834	21.594	24.615	26.186	27.902	29.474	31.491

4.6 Summary

To verify the proposed solutions for more accurate Legendre moment computing in Chapter 3, we have examined the image reconstructions in this section.

Both square and rectangle images, sized at 256×256, 88×256, and 256×174 with 256 gray levels are employed as testing images in this research. We have reconstructed all testing images with Legendre moments up to 240 and with various $k \times k$ numerical schemes. The Peak Signal to Noise Ratio (PSNR) was used as the measurements to evaluate the image reconstruction performance. Overall, the image reconstructions from the proposed more accurate Legendre moment computing are very encouraging.

In general, the PSNR values of reconstructed Figure 4.1 (b) and (d) are higher than those of Figure 4.1 (a) and (c). This reflects the fact of Figure 4.1 (b) and (d) contain less detail information and can be reconstructed accurately with lower orders of Legendre moments.

It needs to be noted that to achieve high accuracy of moment computing, the efficiency issue is one of the biggest challenges. In our experiment, it takes about 170 hours computing time to reconstruct a 256×256 image from the Legendre moments of order 240 with the 11×11 numerical scheme.

Chapter 5

Image Reconstruction from a Partial Set of Legendre Moments

5.1 Introduction

According to the general moment theory expressed in Chapter 2, for a digital image, the lower order moments represent its fundamental features while the higher order moments characterize its details. Based on the previously presented moment computation techniques and precisely reconstructed images, we are able to investigate the individual contributions by a partial set

of Legendre moments.

To examine the image reconstructions determined by a limited band of Legendre moments, we adapt the formula

$$\widehat{f}_{band}(x,y) = \sum_{m=M_{min}}^{M_{max}} \sum_{n=0}^{m} \widehat{\lambda}_{m-n,n}\, P_{m-n}(x)\, P_n(y) \tag{5.1}$$

to perform the image reconstructions. In (5.1), M_{max} and M_{min} denote the highest and lowest orders of Legendre moments involved in image reconstructions. The same two testing images shown in Figure 4.1 (a) and (b) are utilized in this section.

5.2 Image Reconstruction with Different Band of Legendre Moments

The sub-figures (a) to (d) of Figure 5.1 show the images of the reconstructed Figure 4.1 (a) from partial sets of Legendre moments of orders 0 to 40, 41 to 80, 81 to 120, and 121 to 200. The numerical scheme $k = 11$ is adopted to compute Legendre moments in this experiment. Figure 5.1 (e) presents the reconstructed image of orders 0 to 200, and Figure 5.1 (f) displays the result of direct addition operation of images Figure 5.1 (a) to (d). All sub-figures illustrated in Figure 5.1 are the direct reconstructed results without any image enhancement for display. As expected, the images presented in Figure 5.1 (e) and Figure 5.1 (f) are identical.

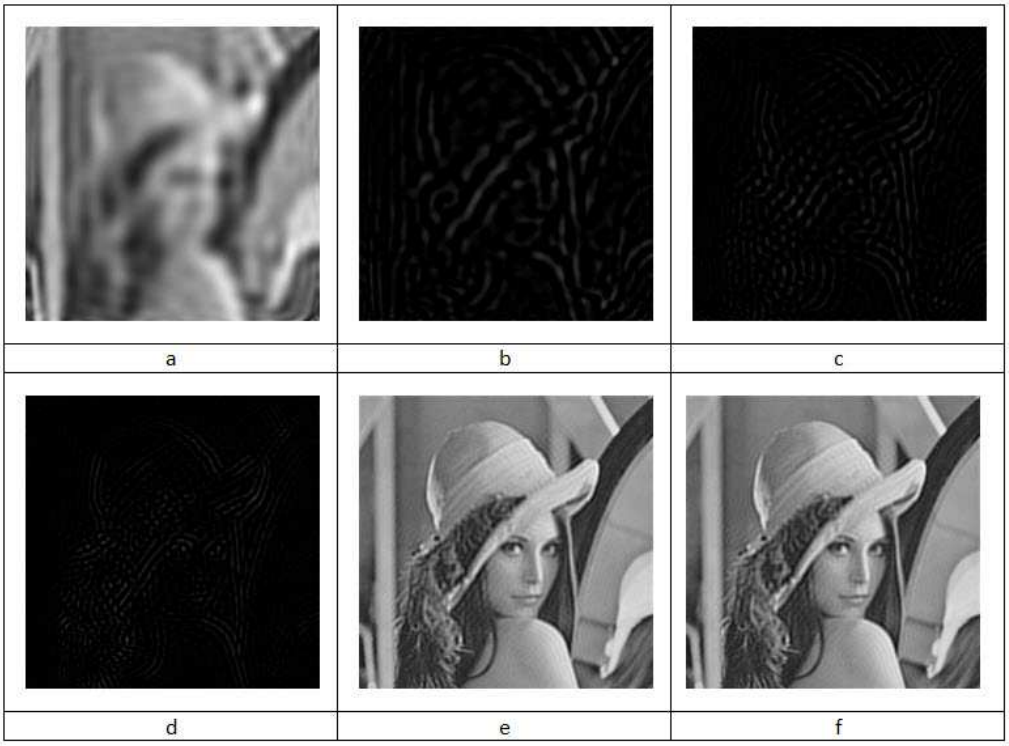

Figure 5.1: Sub-figures (a) to (f) are the reconstructed images of Figure 4.1 (a), with applying 11 x 11 numerical scheme, from Legendre moments of orders 0 to 40, 41 to 80, 81 to 120, 121 to 200, 0 to 200, and the direct addition operation of images (a) to (d).

The results shown in Figure 5.1 have clarified the general moment theory that the lower order Legendre moments represent fundamental features of an image, while the higher order Legendre moments describe its details.

To address the issue of image reconstruction from a partial set of Legendre moments further, we have conducted more investigations with the testing image Figure 4.1 (b).

Figure 5.2 shows some reconstructed images from using lower order of

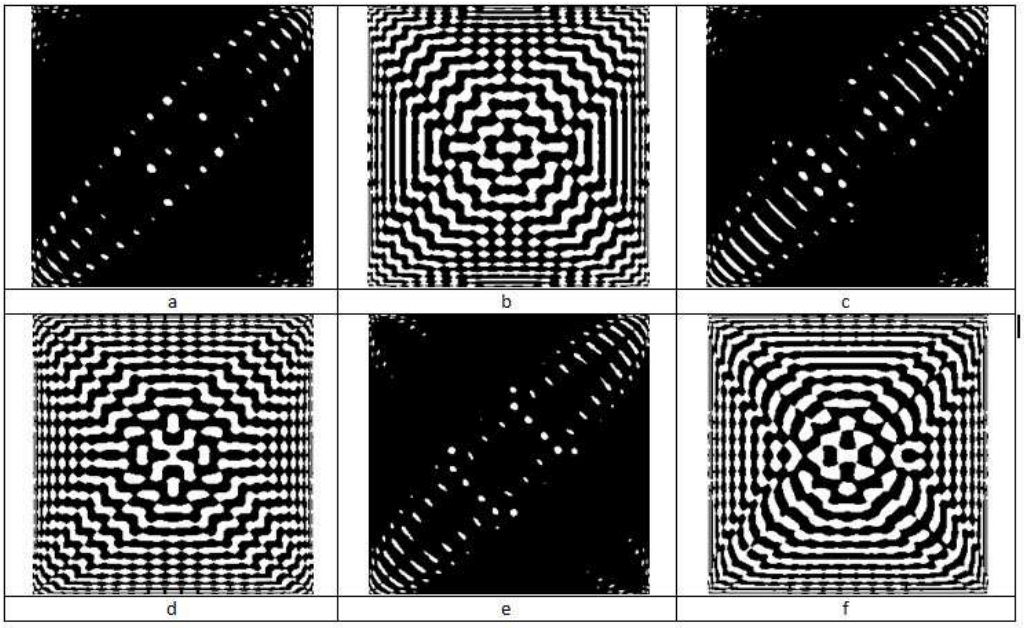

Figure 5.2: Sub-figures (a) to (f) are the reconstructed images of Figure 4.1 (b), with applying 11×11 numerical scheme, from Legendre moments of orders 51, 52, 53, 54, 55, and 51 to 55. The gray levels of all image pixels are multiplied by 10.

individual Legendre moments, 51, 52, 53, 54, 55, and the set of 51 to 55. The histograms of those reconstructed images show that all of the image pixels have gray level values of 25 or less. For a better display of image details, we have re-scaled these images using a multiplier of 10.

Figure 5.3 shows some images reconstructed by using higher order of individual Legendre moments, 196, 197, 198, 199, 200, and the set of 196 to 200. Since the highest gray level of all images is 9, a multiplier of 25 is applied for display.

From the experimental results shown in Figure 5.2 and Figure 5.3, we

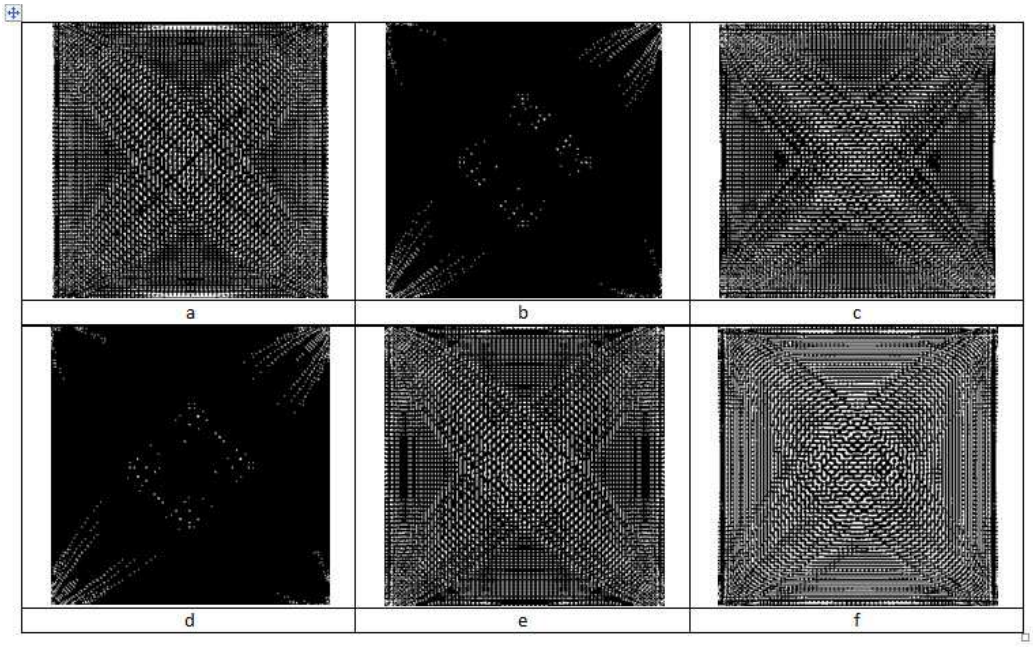

Figure 5.3: Sub-figures (a) to (f) are the reconstructed images of Figure 4.1 (b), with applying 11×11 numerical scheme, from Legendre moments of orders 196, 197, 198, 199, 200, and 196 to 200, respectively. The gray levels of all image pixels are multiplied by 25.

have made some observations about the characteristics of individual orders of Legendre moments in image representation. First, each individual order of moments represents the unique image details independently. Second, the even orders of Legendre moments describe more image details than the odd orders of Legendre moments do. To emphasize this discovery, we have conducted the image reconstructions from all even and odd orders of Legendre moments between 0 and 240, and displayed the results in Figure 5.4 (a) and Figure 5.4 (b).

We can observe that Figure 5.4 (b) has presented very limited information

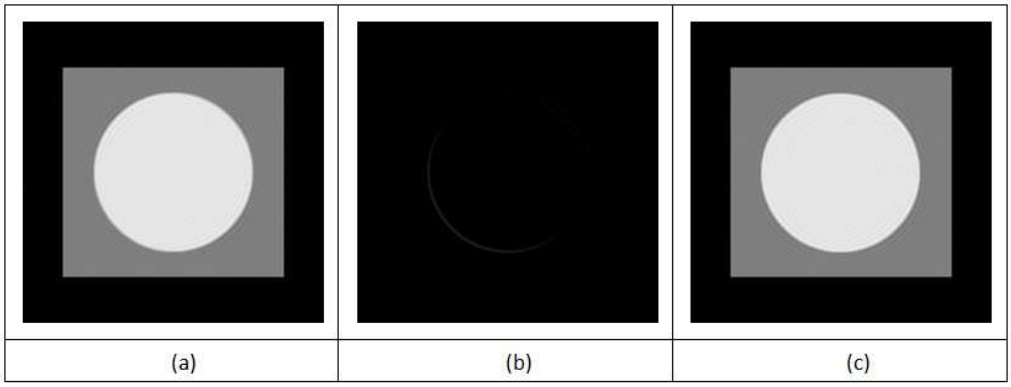

Figure 5.4: Images reconstructed from (a) all even number orders 0 to 240, (b) all odd number orders from 1 to 239, and (c) all orders from 0 to 240.

from the original testing image Figure 4.1 (b). The PSNR value between Figure 5.4 (b) and Figure 5.4 (c) is 6.061. On the other hand, the PSNR value between Figure 5.4 (a) and Figure 5.4 (c) is 39.219, which indicates that the similarity of an image reconstructed from even orders and that of all orders of Legendre moments is very high.

To address this interesting characteristic of Legendre moments further, we have conducted the image reconstructions from the even orders of Legendre moments only. Figure 5.5 presents some reconstructed Figure 4.1 (b) from the even orders of Legendre moments. Compared with each of the sub-figures displayed in Figure 4.4, the two sets of reconstructed images appear very similar. Figure 5.6 shows the PSNR values calculated from the image reconstructions displayed in both of Figure 4.4 and Figure 5.5.

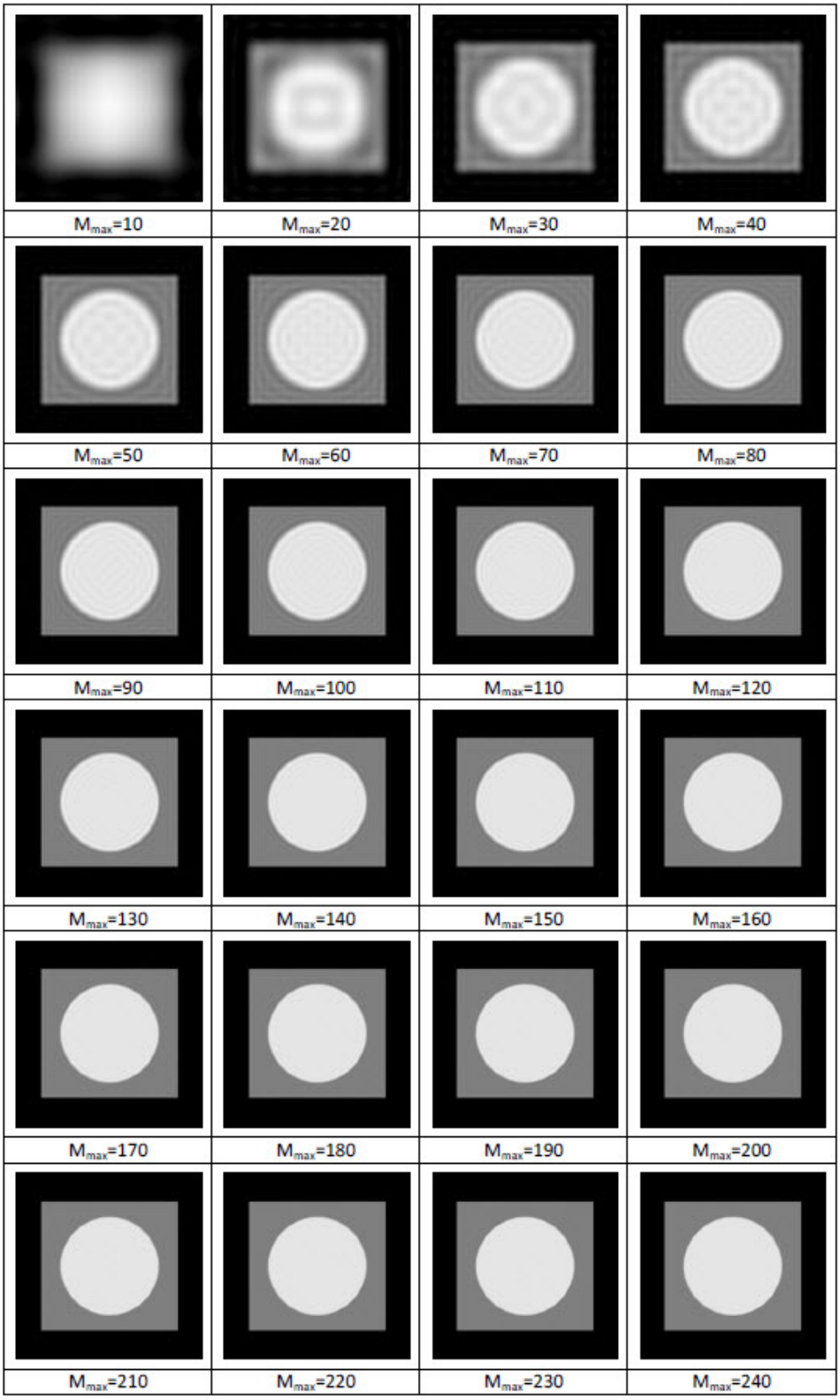

Figure 5.5: Images reconstructed from different even orders of Legendre moments with the 11×11 numerical scheme on Figure 4.1 (b).

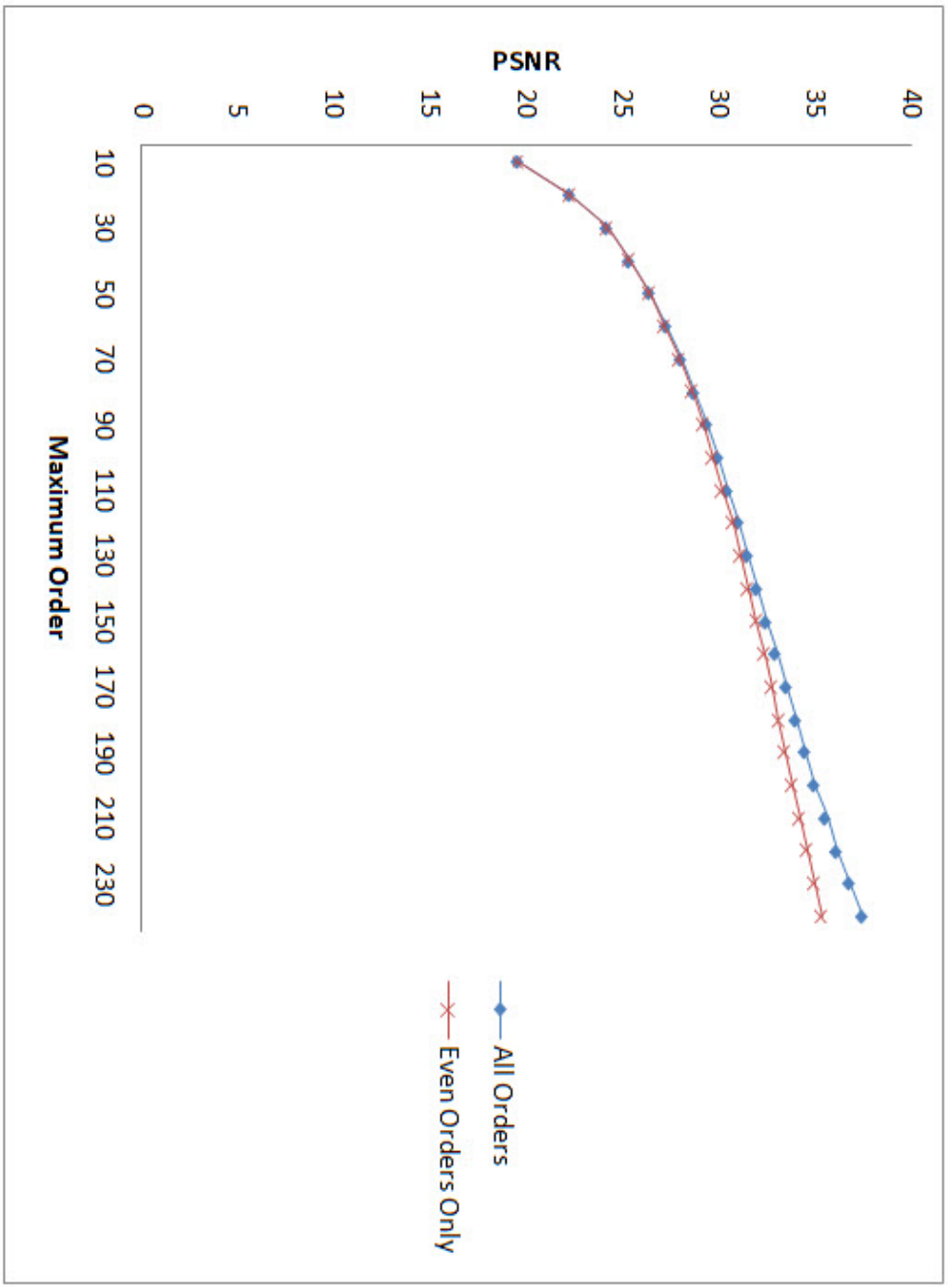

Figure 5.6: PSNRs of the reconstructed Figure 4.1 (b) displayed in Figure 4.4 and Figure 5.5.

5.3 Image Reconstruction with Different Sets of Legendre Moments

In this section, we will discuss the results of experiment that will demonstrate the theory of image projection discussed in Chapter 2. Figure 5.7 and Figure 5.8 show the subset of Legendre moments with $m - n = 0$ and $n = 0$. The results of applying different subsets of Legendre moments to reconstruct Figure 4.1 (b) are represented in Figure 5.9.

We can observe the contribution of subset Legendre moments from $m - n = 0$ projects different direction as from $n = 0$. Futher more on diffferent subset Legendre moments like $m - n = 1$ vs $n = 1$ and $m - n = 2$ vs $n = 2$ also present the same characteristic.

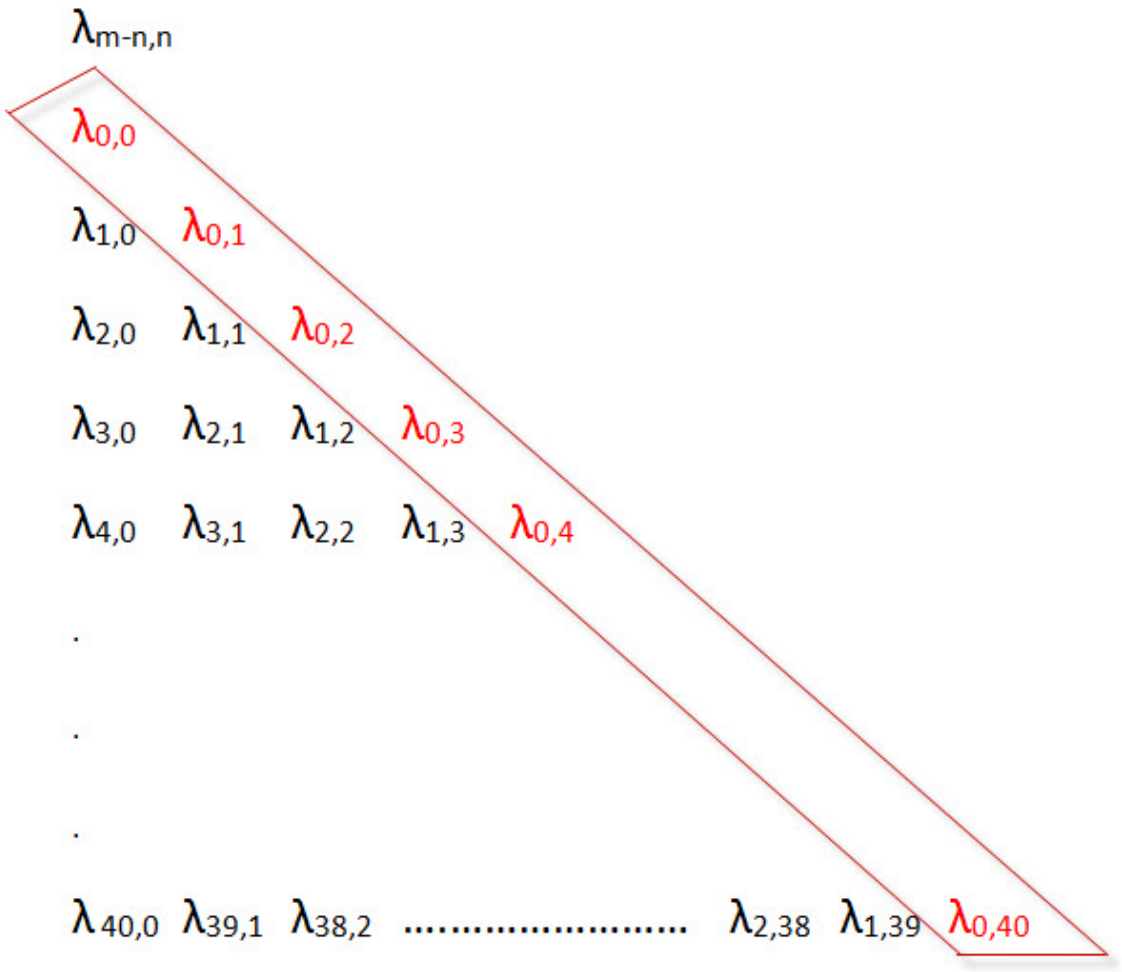

Figure 5.7: A set of λ Values for m-n=0 when minimum order = 0 and maximum order = 40

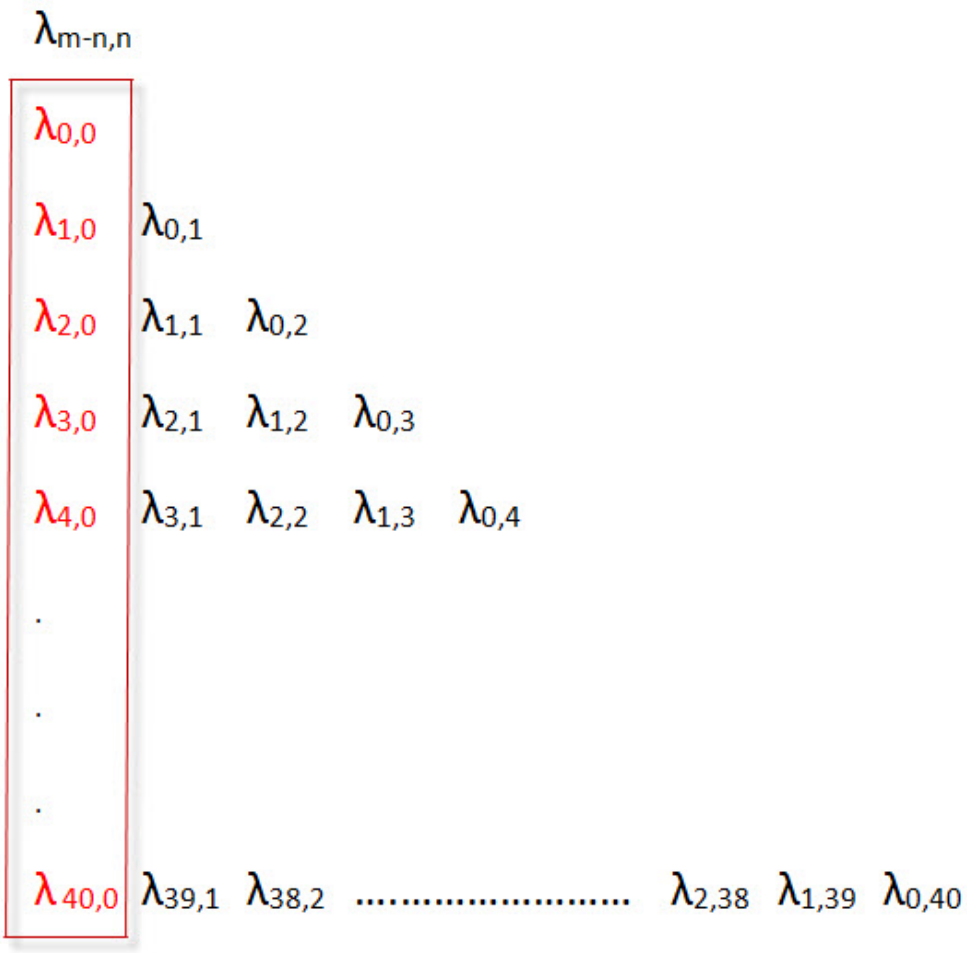

Figure 5.8: A set of λ Values for n=0 when minimum order = 0 and maximum order = 40

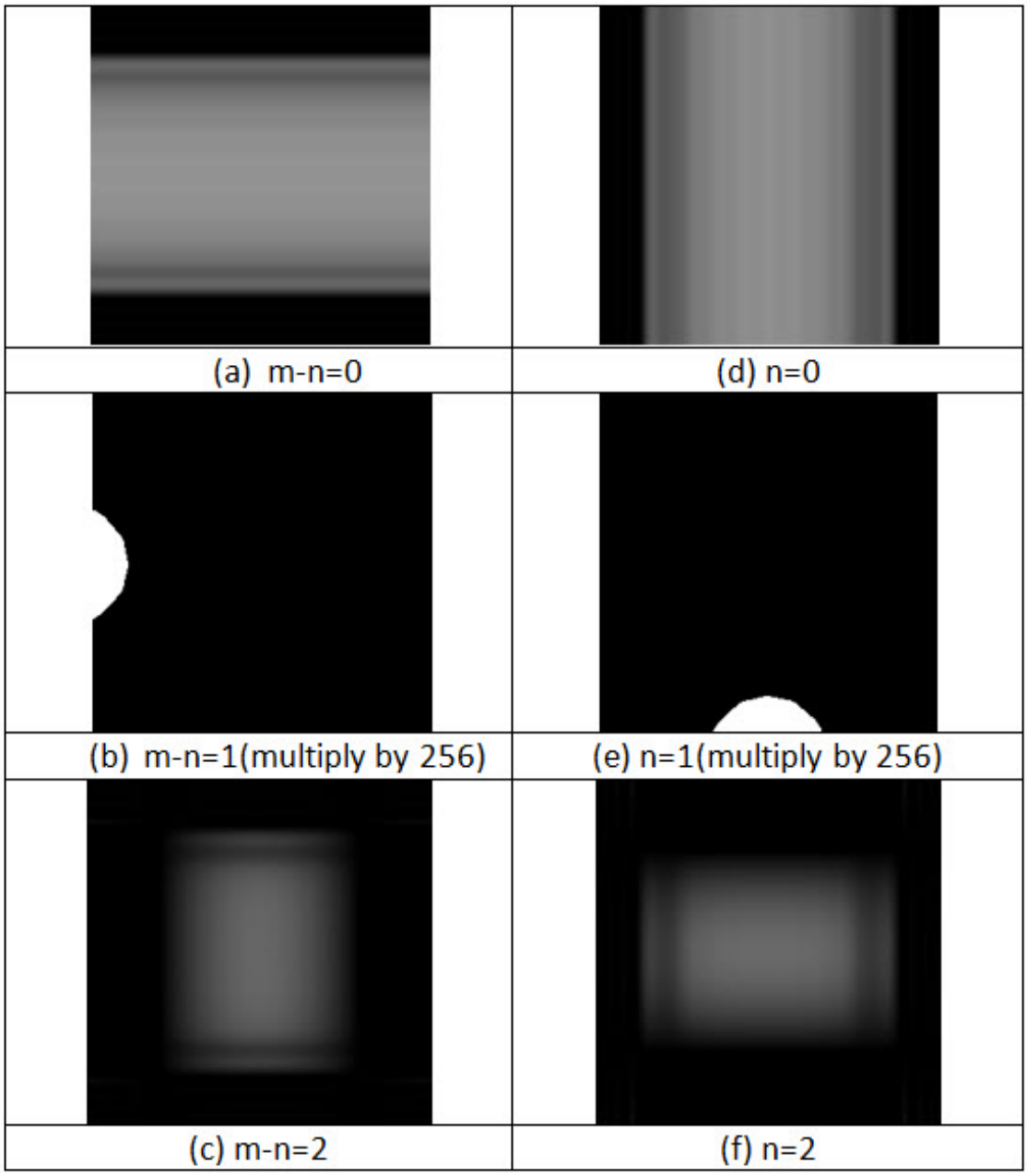

Figure 5.9: Image reconstructed with 1×1 numerical scheme on Minimum order 0 and Maximum Order 40 by applying different set of λ Values on Figure 4.1 (b) followed by different m-n or n values.

5.4 Summary

In this section, we have clarified that every Legendre moment value preserves different information of the original image function, meaning that Legendre moments give the feature of different moment orders describing different parts of the image [12]. The lower order Legendre moments represent the basic fundamental features, while the higher order Legendre moments emerge image details.

We have also discovered an interesting and important Legendre moment characteristics that the even orders of moments contain most of image details.

Furthermore, we have conducted image reconstructions by adopting combination of different Legendre moment subsets and clarified the concept of image projection described in Chapter 2.

Chapter 6

Conclusions and Future Study

6.1 Conclusions

In this research, an innovative attempt was used to improve the computational accuracy of Legendre moments was conducted. Based on the more accurate computed Legendre moments, we have analyzed digital images with the Legendre moments.

To examine the more accurately computed Legendre moments, we have performed image reconstructions from higher orders of Legendre moments with satisfactory results.

By conducting image reconstructions from a partial set of Legendre moments, we have clarified that the lower orders of moments mainly contain the fundamental information of the original image, while the higher orders moments preserve the detailed image information.

We have concluded that each individual finite set of Legendre moments will represent unique image details independently.

We have also discovered that the even orders of Legendre moments describe most of the image characteristics, while the odd orders of Legendre moments would only present very limited information from the original image.

Although the Legendre moments were studied in this research, the detected representing characteristics of individual moments in image analysis are also expected to be present in other conventional continuous orthogonal moments as well.

6.2 Future Study

Even though the results from this thesis have demonstrated the efficient and accurate approach for image reconstruction using Legendre moments, it could be extended further in some ways. Here are some recommendations for future studies.

Extending our approaches in this research to other orthogonal moments

Legendre moment is only one of the important orthogonal moments. In principle, other orthogonal moments, particularly the moments defined in a rectangular region, will very likely have some similar image representation

characteristics. Applying our approaches to other orthogonal moments may produce some similar results as we have discovered in this research.

Improving computational efficiency

One of the major issues that limits our work in this research is the long computing time for many of our moment computational experiments. If researchers can develop new computational algorithms to use graphics processing units (GPUs) in moment calculation processing, it will improve the efficiency of Legendre moment computing substantially. If there is breakthrough on this issue, more new results on the investigation of Legendre moment are highly expected.

Bibliography

[1] Amy Chiang and Simon Liao. Image analysis with legendre moment descriptors. *Journal of Computer Science*, 2014.

[2] Amy Chiang and Simon Liao. Image reconstruction from legendre moments. *The 2014 Annual Conference on Practical Information Management*, 2014.

[3] Richard Courant and David Hilbert. *Methods of mathematical physics*, volume 1. Wiley. com, 2008.

[4] Brian P Flannery, William H Press, Saul A Teukolsky, and William Vetterling. Numerical recipes in c. *Press Syndicate of the University of Cambridge, New York*, 1992.

[5] J. Flusser, T. Suk, and B. Zitova. *Moments and moment invariants in pattern recognition*. John Wiley & Sons, Ltd, 2009.

[6] Rafael C. Gonzalez and Richard E. Woods. *Digital Image Processing, Third Edition*. Pearson Education, Inc, 3 edition, 2008.

[7] B.K.P Horn. Robot vision. *The MIT Press*, 1986.

[8] M. K. Hu. Visual pattern recognition by moment invariants. *IRE Transactions on Information Theory*, 8:179–187, 1962.

[9] S. Liao and M. Pawlak. On image analysis by moments. *IEEE transaction on pattern analysis and machine intelligence*, 18(3):254–266, 1996.

[10] Simon Liao. *Accuracy Analysis of Moment Functions*, volume 1. Science Gate Publishing, 2014.

[11] R. Mukundan and K.R. Ramakrishnan. *Moment Functions in Image Analysis - Theory and Applications*. World Scientific, 1998.

[12] George A. Papakostas. *Over 50 Years of Image Moments and Moment Invariants*, volume 1. Science Gate Publishing, 2014.

[13] Miroslaw Pawlak. *Image Analysis by Moments: Reconstrcution and Aomputational Aspects*. Oficyna Wydawnicza Politechniki WrocLawskiej, WrocLaw, 2006.

[14] G Sansone. *Orthogonal functions*, volume 9. Dover Publications, 1991.

[15] G. Szegö. *Orthogonal Polynomials*. American Mathematical Society Colloquium Publications, Providence, R.I., 1975.

[16] M. R. Teague. Image analysis via the general theory of moments. *Opt. Soc. Am.*, 70:920–930, 1980.

[17] C. H. Teh and R. T. Chin. On digital approximation of moment in invariants. *Computer vision, graphics and image processing*, 33(3):318–326, 1986.

[18] C. H. Teh and R. T. Chin. On image analysis by the methods of moments. *IEEE transactions on pattern analysis and machine intelligence*, 10(4):496–513, 1988.

[19] Xiaoyu Wang and Simon Liao. Image reconstruction from orthogonal fourier-mellin moments. In *Image Analysis and Recognition*, pages 687–694. Springer, 2013.